Implementing and Evaluating Variable Soil Thickness in the Community Land Model, Version 4.5 (CLM4.5)

MICHAEL A. BRUNKE,* PATRICK BROXTON,* JON PELLETIER,+ DAVID GOCHIS,# PIETER HAZENBERG,* DAVID M. LAWRENCE,# L. RUBY LEUNG,@ GUO-YUE NIU,& PETER A. TROCH,& AND XUBIN ZENG*

* *Department of Atmospheric Sciences, The University of Arizona, Tucson, Arizona*
+ *Department of Geosciences, The University of Arizona, Tucson, Arizona*
# *National Center for Atmospheric Research, Boulder, Colorado*
@ *Pacific Northwest National Laboratory, Richland, Washington*
& *Department of Hydrology and Water Resources, The University of Arizona, Tucson, Arizona*

(Manuscript received 20 April 2015, in final form 31 October 2015)

ABSTRACT

One of the recognized weaknesses of land surface models as used in weather and climate models is the assumption of constant soil thickness because of the lack of global estimates of bedrock depth. Using a 30-arc-s global dataset for the thickness of relatively porous, unconsolidated sediments over bedrock, spatial variation in soil thickness is included here in version 4.5 of the Community Land Model (CLM4.5). The number of soil layers for each grid cell is determined from the average soil depth for each 0.9° latitude × 1.25° longitude grid cell. The greatest changes in the simulation with variable soil thickness are to baseflow, with the annual minimum generally occurring earlier. Smaller changes are seen in latent heat flux and surface runoff primarily as a result of an increase in the annual cycle amplitude. These changes are related to soil moisture changes that are most substantial in locations with shallow bedrock. Total water storage (TWS) anomalies are not strongly affected over most river basins since most basins contain mostly deep soils, but TWS anomalies are substantially different for a river basin with more mountainous terrain. Additionally, the annual cycle in soil temperature is partially affected by including realistic soil thicknesses resulting from changes in the vertical profile of heat capacity and thermal conductivity. However, the largest changes to soil temperature are introduced by the soil moisture changes in the variable soil thickness simulation. This implementation of variable soil thickness represents a step forward in land surface model development.

1. Introduction

Land surface models (LSMs) are utilized by general circulation models (GCMs) to represent land surface processes, primarily for the purpose of modeling land–atmosphere interactions as represented by energy and water fluxes across the land–atmosphere interface. When coupled to river transport models (RTMs), LSMs can also represent the transport of water from land back to the ocean. Accurate modeling of soil moisture is a prerequisite for a good representation of land–atmosphere interactions and surface runoff (Liang et al. 2003). Both of these require an accurate representation of groundwater. Gravity and capillary forces create water fluxes between the unsaturated soil and groundwater (Niu et al. 2007). Thus, a shallow water table would have more of an effect on the soil moisture profile than a deep one (Chen and Hu 2004). Shallow water tables also provide water for evapotranspiration and are more likely to result in runoff from saturation excess (Gutowski et al. 2002; York et al. 2002; Liang et al. 2003; Chen and Hu 2004). In fact, runoff was found to be more related to water table depth than to precipitation (Eltahir and Yeh 1999). Additionally, shallow water tables have been shown to impede drainage, creating wetlands in regions unaffected

Supplemental information related to this paper is available at the Journals Online website: http://dx.doi.org/10.1175/JCLI-D-15-0307.s1.

Corresponding author address: Michael A. Brunke, Department of Atmospheric Sciences, The University of Arizona, P.O. Box 210081, Tucson, AZ 85721-0081.
E-mail: brunke@atmo.arizona.edu

DOI: 10.1175/JCLI-D-15-0307.1

by seasonal flooding (Miguez-Macho and Fan 2012). Fan et al. (2013) found that 22%–32% of land globally is affected by shallow groundwater. Groundwater provides a source of water for evapotranspiration even during dry seasons or drought conditions (Yeh et al. 1998; Gutowski et al. 2002; Miguez-Macho and Fan 2012). In fact, some plants are highly reliant on groundwater (Orellana et al. 2012; Rossatto et al. 2012). Roots have been documented down to around 18 m in the Amazon (Nepstad et al. 1994) and even deeper elsewhere (Canadell et al. 1996). Fan et al. (2013) estimated that the water table was high enough to be used by plants in between 7% and 17% of global land.

A widespread practice to model groundwater is to implement a model to represent the groundwater that interacts with a soil moisture column of constant depth globally. Some models (e.g., Gutowski et al. 2002; York et al. 2002) explicitly model the three-dimensional flow of groundwater, but these are computationally expensive to implement into GCMs (York et al. 2002). These have largely been implemented into regional models with finer horizontal resolution since horizontal transport is more important at these smaller scales (York et al. 2002; Yeh and Eltahir 2005). Others implement a simplified one- (e.g., Liang et al. 2003; Niu et al. 2007; Yeh and Eltahir 2005; Koirala et al. 2014) or two-dimensional (e.g., Miguez-Macho et al. 2007) representation of groundwater. One of these simpler representations (Niu et al. 2007) is currently included in the Community Land Model, version 4.5 (CLM4.5; Oleson et al. 2013). It is connected to a soil column of a constant depth of 3.8 m. Within the soil column, soil moisture is found using the revised Richards equation of Zeng and Decker (2009). This revision allows the soil-moisture-based version of the Richards equation to be used under saturated conditions as would be found when the water table lies within the soil column, so that a separate groundwater model may not be necessary. Decker and Zeng (2009) suggested that the separation of soil moisture processes and groundwater is unrealistic and physically unjustified and further showed how this revision of the Richards equation (with the groundwater model removed) improved CLM3.5. Still, the thickness of the soil column was held constant at around 3.5 m.

However, soil thickness varies from region to region. Uplands tend to have shallow soil thicknesses, while lowlands have deeper soils. In uplands, soil depths vary from slope to slope because of differences between rates of soil production and erosion, which depend on terrain slope, climate, and rock type (Pelletier and Rasmussen 2009). In principle, variable soil thickness in LSMs should make the models more realistic, but implementation has been impractical because of a lack of global estimates of bedrock depth. Instead, localized estimates have been more prevalent. For instance, Dietrich et al. (1995), Roering (2008), Pelletier and Rasmussen (2009), and Tesfa et al. (2009) developed geomorphically based soil depth models, applying them to upland basins.

Including variations in soil thickness is an important next step in LSM evolution. Soil thickness is the main determinant of hydrologic response in upland watersheds since thin soils are more likely to produce surface runoff than thicker soils which can store more water (Pelletier and Rasmussen 2009). Soil depth has been shown to control infiltration rates in a desert basin in Nevada (Woolhiser et al. 2006). When the soil column thickness was reduced to realistic values in the Noah LSM for selected locations in the mountains of semiarid northwest Mexico, there was more variation in simulated half-hourly latent heat fluxes over the summer (Gochis et al. 2010). However, soil thickness may not have a large impact on model simulations in all regions or in all model configurations, as Gulden et al. (2007) showed that a deeper soil column containing 30 layers is equally adept at representing column total water storage in Illinois as the 10-layer CLM coupled with the unconfined aquifer model.

The use of variable soil thickness in LSMs has been hampered by the lack of any global estimate of such a quantity. Building upon the partial success of previous localized attempts at soil depth generation, Pelletier et al. (2016) have developed a 30-arc-s (~1 km) global dataset of the thickness of relatively porous, unconsolidated sediments over bedrock (essentially soil thickness) based on topographic, geologic, and climate data. Separate models for upland hillslopes and valley bottoms/lowlands are utilized. Globally, lowlands are determined from geologic data and topographic criteria. Lowland soil thickness is simply predicted using a model that is based on topographic curvature that is calibrated with high-density well data from four U.S. states. Valley bottoms that exist in upland landscapes are determined using topographic analysis (Pelletier 2013), and the thickness of soil/alluvium for a particular valley bottom is predicted from the curvature of the valley bottom and the gradient of the hillslopes flanking the valley. Soil thickness on the remaining upland hillslopes is then predicted by a geomorphic model that balances soil production with erosion. It is based on topographic curvature but has parameters that are dependent on climate, which are calibrated with soil data from the State Soil Geographic (STATSGO) database across the contiguous United States (Miller and White 1998). This dataset contains separate soil thickness estimates for

uplands and lowlands along with the fraction of lowland/upland within each 30-arc-s pixel.

The calibration and evaluation data for the dataset are primarily from midlatitude sites, so their quality in tropical and polar regions is more uncertain than in the midlatitudes. The distinction between shallow and deep soils is also largely influenced by geologic mapping. The quality of these maps is highest in North America (where the data are at higher resolution) and regions of the world where there has been significant oil and gas exploration. The predicted soil depths for areas with shallow soils (which would potentially influence results here) are found to be within 80 cm of those indicated by independent validation data on a different continent than the calibration data a majority (>80%) of the time. More information about the techniques and data used to construct the dataset, as well as calibration and validation of the models are provided in Pelletier et al. (2016).

The previous small-scale studies motivate us to investigate what would happen when global soil depth is implemented into an LSM. We hypothesize that the LSM would be more sensitive to a variable soil thickness in places where bedrock is shallow, as was found by Gochis et al. (2010), but simulations with deep bedrock would be similar to existing simulations using a groundwater model, like what Gulden et al. (2007) found. Here, we document the implementation of the global soil thickness into the latest version of CLM, CLM4.5. Section 2 describes how groundwater processes are handled currently in CLM4.5 and the changes that are made here to include variable soil thickness. The various sensitivity tests carried out to evaluate the performance of variable soil thickness are explained in section 3, and the results of these sensitivity tests are given in section 4. Finally, these results are summarized and further discussed in section 5.

2. The model

a. *The current representation of hydrological processes in CLM4.5*

The current configuration of CLM4.5 is shown in the left panel of Fig. 1. It includes an unconfined aquifer (Niu et al. 2007) that is positioned below a 10-layer soil column of a constant depth of around 3.8 m. A maximum of 5000 mm of water is allowed in the unconfined aquifer (Oleson et al. 2013). If the unconfined aquifer reaches this maximum, the water table is allowed to be within the soil column. In this case, a recharge rate is defined by Darcy's law:

$$q_{\text{recharge}} = -k_{\text{aq}} \frac{\psi_{\nabla} - \psi_{\text{jwt}}}{z_{\nabla} - z_{\text{jwt}}}, \tag{1}$$

where $\psi_{\nabla} = 0$ is the soil matric potential at the water table depth z_{∇}, ψ_{jwt} is the soil matric potential in the layer above the water table, and z_{jwt} is the depth of the layer above the water table. Furthermore, k_{aq} is a hydraulic conductivity of recharge that is based on the hydraulic conductivity of the layer that contains the water table depth (jwt + 1) such that $k_{\text{aq}} = \Theta_{\text{ice,jwt+1}} k(z_{\text{jwt+1}})$ with $\Theta_{\text{ice,jwt+1}}$ being an ice impedence factor for that layer such that

$$\log\Theta_{\text{ice}} = -6 \left(\frac{\sum_{i=\text{jwt}}^{10} F_{\text{ice},i} \Delta z_i}{\sum_{i=\text{jwt}}^{N_{\text{levsoi}}} \Delta z_i} \right), \tag{2}$$

where $F_{\text{ice},i}$ is the fraction of pore space filled with ice. The change in water table depth is a function of how much water is added to the unconfined aquifer by recharge q_{recharge} and how much is removed by drainage q_{drain}:

$$\Delta z_{\nabla} = \frac{q_{\text{recharge}} - q_{\text{drain}}}{S_y} \Delta t, \tag{3}$$

where Δt is the model time step. The specific yield S_y is defined as

$$S_y = \theta_{\text{sat}} \left[1 - \left(1 + \frac{z_{\nabla}}{\psi_{\text{sat}}} \right)^{-1/B} \right], \tag{4}$$

where θ_{sat} and ψ_{sat} are the saturated values of volumetric soil moisture and soil matric potential, respectively, and B is the Clapp–Hornberger exponent. The subsurface drainage q_{drain} is based upon Niu et al. (2005) with the addition of the ice impedence factor:

$$q_{\text{drain}} = \Theta_{\text{ice}} q_{\text{drain}_{\text{max}}} \exp(-f_{\text{drain}} z_{\nabla}), \tag{5}$$

where $q_{\text{drain}_{\text{max}}}$ is a maximum drainage rate based upon the mean gridcell topographic slope β such that $q_{\text{drain}_{\text{max}}} = 10 \sin\beta$ and f_{drain} is a decay factor of 2.5 m^{-1}.

In the case of the water table lying below the model soil column, the aquifer water storage is less than 5000 mm, and the recharge rate is based upon a hypothetical soil layer between the bottom of the explicit soil column in layer N_{levsoi} and the top of the unconfined aquifer (Zeng and Decker 2009):

$$q_{\text{recharge}} = \frac{\Delta\theta_{\text{liq},N_{\text{levsoi}}+1} \Delta z_{N_{\text{levsoi}}+1}}{\Delta t}, \tag{6}$$

where $\Delta\theta_{\text{liq},N_{\text{levsoi}}+1}$ is the change of liquid water content in this hypothetical layer during a model time step and $\Delta z_{N_{\text{levsoi}}+1}$ is the difference between the water table depth

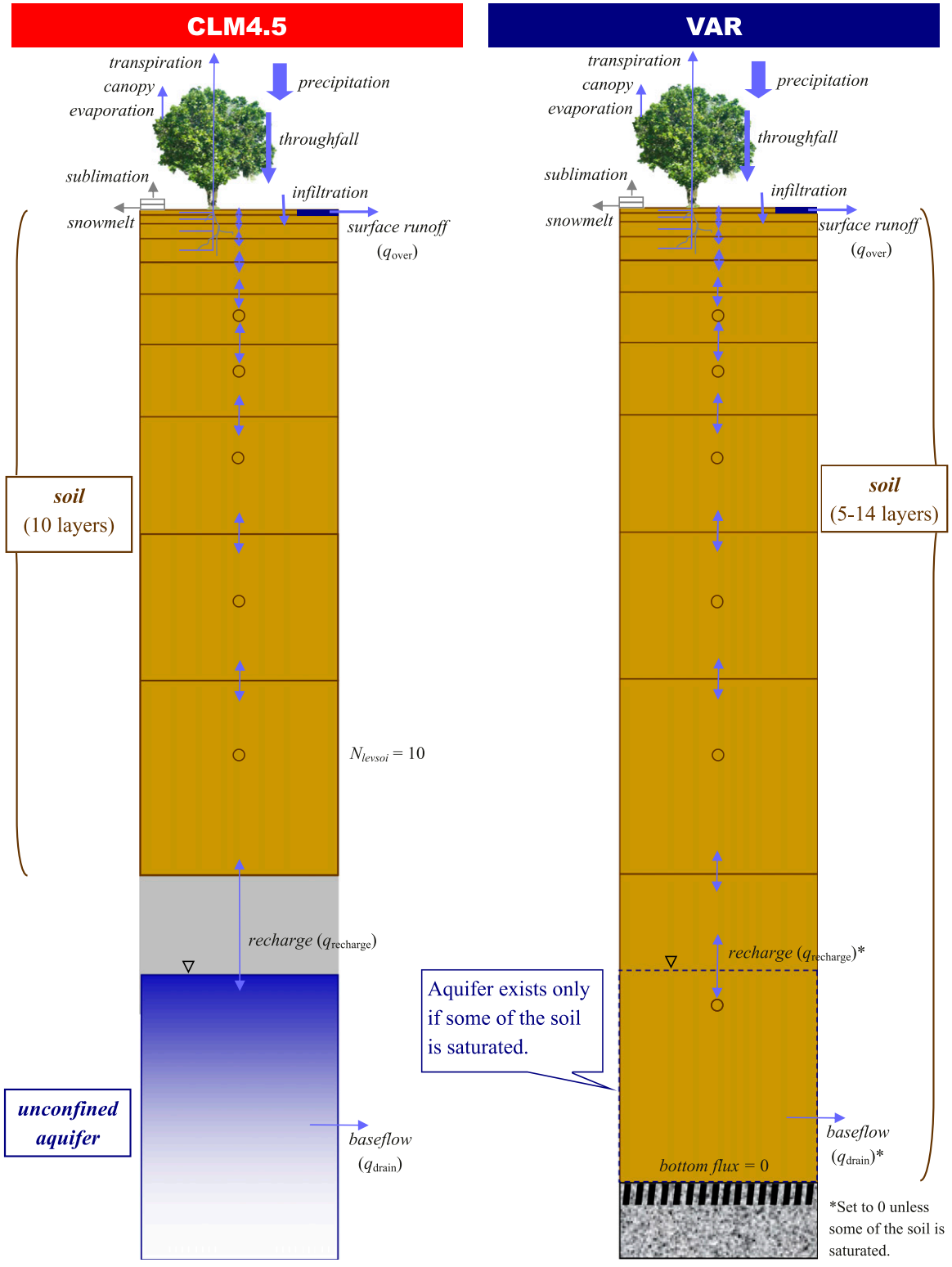

FIG. 1. Hydrological processes (left) considered originally in CLM4.5 and how they are considered in the version (right) with variable soil thickness (VAR). The yellow-brown layers represent the soil column.

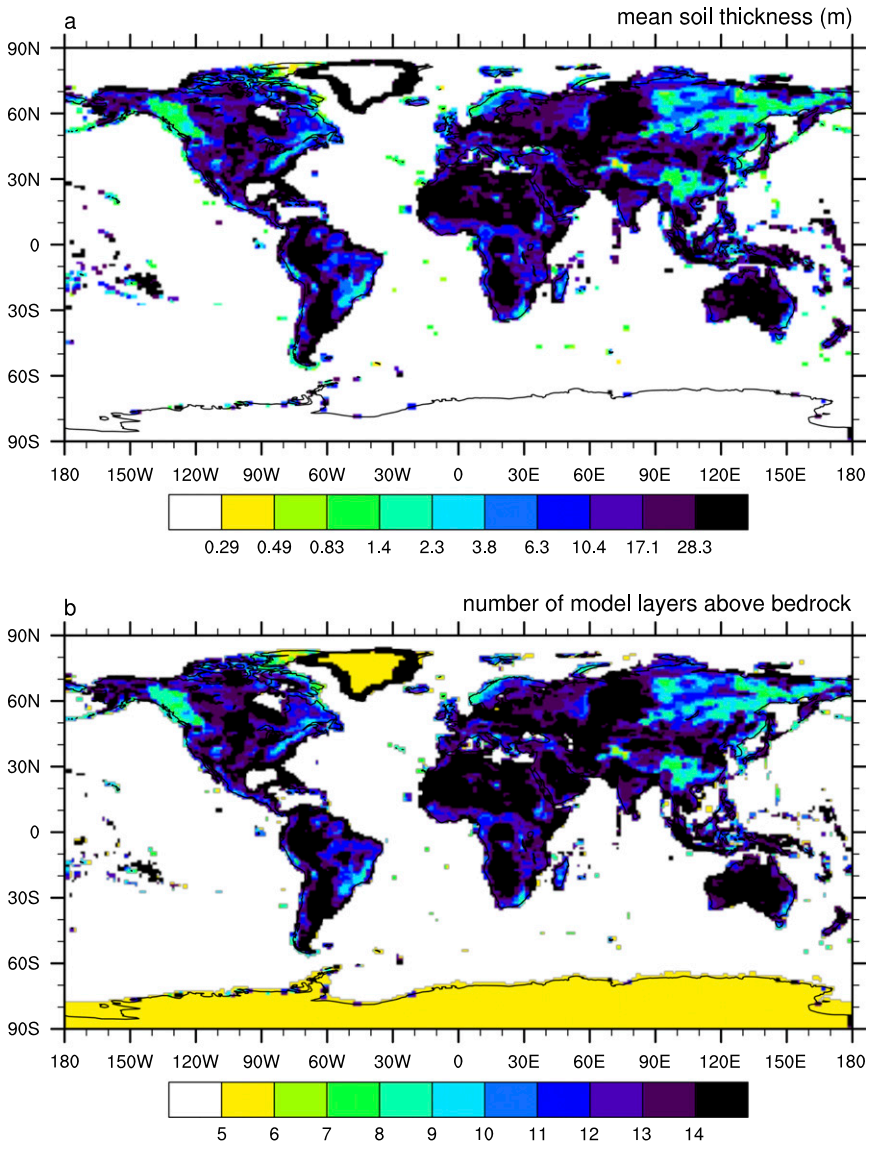

FIG. 2. (a) The dataset soil thickness averaged to the model resolution used here of approximately 0.9° lat × 1.25° lon. (b) The number of hydrologically active CLM layers above bedrock from (a).

z_∇ and the bottom of the soil column $\Delta z_{N_{\text{levsoi}}}$. The change in the amount of water in the unconfined aquifer is given by the following:

$$\Delta W_a = (q_{\text{recharge}} - q_{\text{drain}})\Delta t. \tag{7}$$

b. *How variable soil thickness is accounted for in CLM4.5*

To include variable soil depth, the almost 1-km soil thicknesses within each 0.9° latitude × 1.25° longitude resolution grid cell are averaged to obtain the gridcell average depth to bedrock (DTB). This depth is then used to determine the number of soil layers in each grid cell (Fig. 2a). This is one of a number of ways to aggregate the high-resolution DTB into a single gridcell quantity. For instance, the median DTB for each grid cell could be used to determine the number of soil layers instead. We will briefly explore this possibility for a single grid cell in Colorado with a large intragridcell variability in DTB in section 4.

The ground layer vertical structure in CLM4.5 is maintained, but the number of hydrologically active soil layers is increased or decreased based on average DTB from the standard value of 10. The depth of the node for a particular layer i is determined to be

$$z_i = 0.025[e^{0.5(i-0.5)} - 1], \tag{8}$$

and the bottom of that layer is found by the following:

$$z_{b_i} = \begin{cases} 0.5(z_i + z_{i+1}), & \text{for} \quad i = 1, \ldots, 14 \\ z_{14} + 0.5(z_{15} - z_{14}), & \text{for} \quad i = 15 \end{cases}. \tag{9}$$

The node and bottom interface depths from Eqs. (8) and (9) are given in Table S1 of the supplemental material. A minimum of five layers (corresponding to a soil thickness of ~0.3 m) and a maximum of 14 layers (corresponding to a soil thickness of ~28 m) are allowed. The number of soil layers for a particular grid cell within that range is determined based upon where the 0.9° × 1.25° depth to bedrock happens to fall. If the bedrock depth falls above the middle of a particular layer N, then the model bedrock depth is put at the top of that layer, and there are $N - 1$ soil layers. If the bedrock depth falls at or below the middle of layer N, the model bedrock depth is placed at the bottom of that layer, and there are N layers. Figure 2b shows the number of soil layers allowed in CLM4.5 with variable soil depth globally. This simple change is appropriate in this study because it keeps the model as similar to the original version as possible in order to avoid colluding the effects of introducing variable soil thicknesses from other effects due to model changes. However, we would note that as the thickness of layers grows exponentially with depth, this may introduce limitations when the soil thickness is deep.

As the number of soil layers at each land grid cell extends effectively to bedrock, it is no longer necessary to include an artificial unconfined aquifer below the soil column; therefore, we remove it. Instead, a water table only exists if any of the soil layers become fully or partially saturated (Fig. 1, right). In such a case, recharge is defined as in Eq. (1), and the water table depth changes according to Eq. (3) with the constraint that it cannot be deeper than the bottom of the last soil layer allowed (i.e., the model bedrock depth). An assumption of equilibrium in that bottom soil layer is made so as to determine when water table depth can be above model bedrock depth (see section S1 of the supplemental material). A zero bottom flux boundary is currently assumed, which allows no water to flow into bedrock, but future versions could allow a flow of water into the bedrock if the bedrock porosity and hydraulic conductivity are known. Also, maximum baseflow is determined as in Eq. (5), but the total baseflow cannot exceed that fraction that can be removed from the saturated storage of the soil column.

If a particular soil column has less than the default 10 layers, then the root fractions (Zeng 2001) used in the determination of how much water is removed from each layer by transpiration need to be adjusted. When the number of layers is less than 10, the original root fractions within the number of layers allowed are normalized by the sum of the root fractions calculated for the original 10 layers. For grid cells with 10 or more layers, the root distribution is unchanged, and no roots are allowed in any layer below the tenth soil layer. As the focus of this paper is on the effects of variable soil thickness and not on vegetation, we do this to keep the model as similar to the CLM4.5 release as possible. However, deep roots have been observed in places like the Amazon (Nepstad et al. 1994; Zeng et al. 1998) and may play more of a role in arid and semiarid environments (Canadell et al. 1996). The root fraction distribution might need to be adjusted to account for the possibility of these deep roots in the future. While we ignore the effects of deep roots for now, we perform a sensitivity test of the effect of this assumption that is shown in section 5.

If there are less than 10 layers within a soil column, surface runoff also must be adjusted, since it depends on water table depth:

$$q_{\text{over}} = f_{\max} e^{-0.5 f_{\text{over}}} q_{\text{liq},0} \tag{10}$$

where $q_{\text{liq},0}$ is the flux of water coming from above the soil, f_{over} is a decay factor set to 0.5 m^{-1}, and $f_{\max}$ is the maximum fraction of surface water flux capable of running off if the water table is at the surface ($z_\nabla = 0$). In our new version with variable soil thickness, depth to the water table from the surface cannot exceed the model bedrock depth, because a saturated zone is assumed not to be able to exist below this depth. For shallow soil thicknesses, this constrained z_∇ would be too close to the surface, leading to an overestimation of surface runoff. Therefore in our adapted version, we adjust f_{over} so that the exponent will be near 0 at the model bedrock depth by increasing it such that

$$f_{\text{over}} = 0.5 \frac{3.8\,\text{m}}{z_{\text{bot}}}, \tag{11}$$

where z_{bot} is the model bedrock depth.

3. Sensitivity tests

The principal runs performed here are the unaltered CLM4.5 (referred to as CLM4.5), VAR with the changes to include variable soil depth as described above, and DEEP using the same framework as for VAR but with a constant 14 soil layers globally (down to a depth of ~28.25 m). In other words, model bedrock depth is at the bottom of the 14th layer everywhere in DEEP allowing

the simulation of the unconfined aquifer within the soil column and not by the Niu et al. (2007) formulation with the water table possibly below the bottom of the tenth soil layer in CLM4.5. This last run is performed to help illustrate some of the differences in VAR relative to CLM4.5 that are contributed by the change in the bottom boundary condition of removing the aquifer model and replacing it with zero flux at the bottom interface.

All simulations are run uncoupled to the atmosphere using the Qian et al. (2006) forcing data with satellite phenology of prescribed vegetation characteristics as derived from MODIS. We found that VAR with its deep soil profiles in some grid cells needed about 200 years for the soil moisture and water table to spin up to equilibrium. Additionally, DEEP with its 14 soil layers everywhere would need that same amount of simulation time to spin up. We spin up all the runs, using a repeated Qian et al. (2006) meteorological forcing for 1948–2004. Then, we use the same forcing to perform 50-yr simulations for each experiment. These final runs are what are analyzed in the following sections, focusing mostly on the 20 years corresponding to 1978–97 unless otherwise noted. We also assess the sensitivity of VAR to the forcing used by running it with the forcing that is derived from the Climate Research Unit (CRU) climatology with the diurnal cycle and daily variability of the National Centers for Environmental Prediction (NCEP)–National Center for Atmospheric Research (NCAR) reanalysis (referred to as CRUNCEP forcing). This run (denoted as VARCRU) is spun up in the same way as the other runs. This run will be explored in sections 4c and 5.

To illustrate differences between the simulations, we analyze standard statistics like means and root-mean-square differences (RMSDs). We also analyze mean annual ranges (MARs) with a focus on both the differences in MAR between simulations and the MAR of the differences between simulations. The former would be 0 if there is no amplitude difference in the mean annual cycles of the two runs and is not affected by the phase shift. However, the latter is affected by both phase shifts in the annual cycle and amplitude changes. The statistical significance of the mean differences is found by performing a two-tailed Student's t test.

Also shown in section 4c are the simulated monthly mean total water storage (TWS) anomalies from the simulations compared with those from the Gravity Recovery and Climate Experiment (GRACE) observations. GRACE-derived anomalies based on spherical harmonics from three groups [Chen et al. 2005; Swenson and Wahr 2006; Landerer and Swenson 2012; dataset produced by Swenson (2012), downloaded from http://grace.jpl.nasa.gov] are used to represent data uncertainty. For CLM4.5, the subsurface contribution to TWS is considered to be the sum of the water stored in the unconfined aquifer below the soil column and the integrated water within the soil column. In DEEP and VAR, it is just the integrated water in the soil column since the aquifer does not exist below the soil column in these simulations. For all simulations, TWS also includes snow and surface water. All anomalies are computed from the 2002–04 means.

4. Results

a. *Changes to the mean and interannual variability*

Generally, seasonal means in DEEP surface runoff are only slightly changed compared to CLM4.5 (Fig. 3c and Fig. S1c in the supplemental material). Therefore, the change in bottom boundary condition by removing the unconfined aquifer model has little effect on surface runoff. On the other hand, baseflow can be quite strongly affected by the bottom boundary change in some regions and varying by season as shown in Fig. 3d and Fig. S1d. However, some of these large changes in baseflow are not statistically significant at the 90% level. The reduction of soil layers in VAR compared to DEEP in certain areas such as parts of eastern Siberia, southeastern Asia, and northwestern North America has more of an impact on surface runoff as represented by the statistically significant differences between VAR and DEEP (Fig. 3e and Fig. S1e) and also impacts baseflow quite substantially in some of these same regions (Fig. 3f and Fig. S1f).

Interannual variability in surface runoff and baseflow is also affected in VAR. Figures 4a,b present the median RMSDs of annual mean surface runoff and baseflow between VAR and CLM4.5 for various bins of mean annual range in total precipitation as a function of the number of soil layers used in VAR. The interannual variability of VAR surface runoff and baseflow is higher at locations where the number of soil layers is the same or less than in CLM4.5 and where there is a higher mean annual range in precipitation (Figs. 4a,b). There is also elevated interannual variability of baseflow at some deep bedrock grid cells (number of soil layers >10) if the annual range in rainfall is high enough (Fig. 4b). Comparing this to the median RMSDs between DEEP and CLM4.5, some of the higher variability in baseflow can be explained by the change in bottom boundary especially for the extended soil columns (Figs. 4b,d), whereas very little of the change in variability in surface runoff can be explained by this (Figs. 4a,c). The median RMSDs between VAR and DEEP (Fig. S2 in the supplemental material) look similar to those between VAR and CLM4.5 for shallow soil columns (i.e., number of soil layers ≤ 10) (Figs. 4a,b), confirming that the change

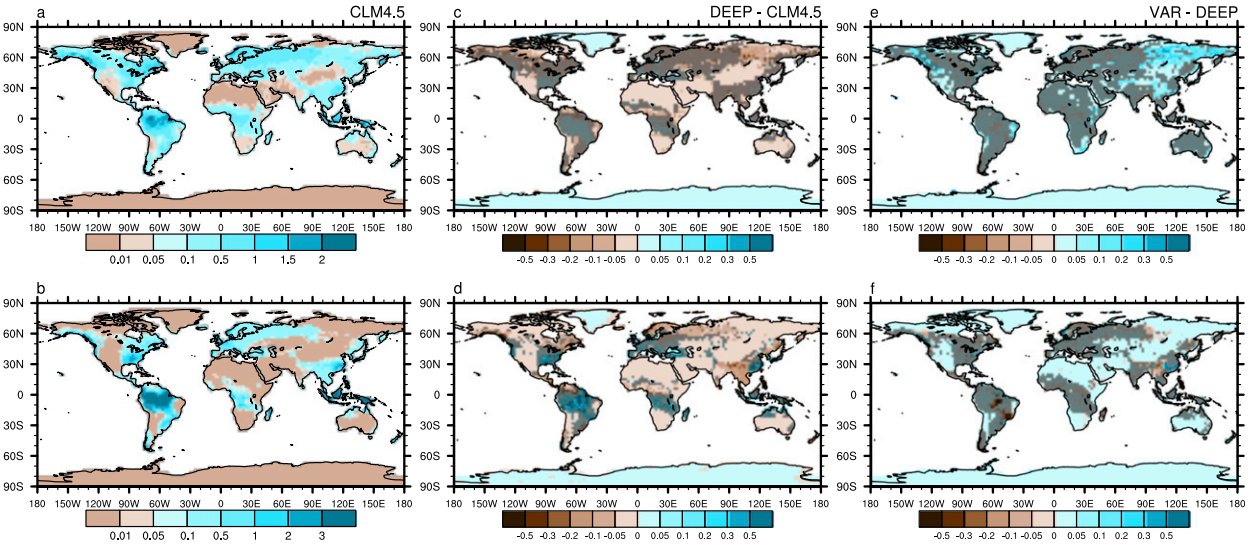

FIG. 3. The March–May seasonal mean (a) surface runoff and (b) baseflow in CLM4.5, (c),(d) the difference in these seasonal means between DEEP and CLM4.5, and (e),(f) the difference in these between VAR and DEEP (mm day^{-1}). The overshading in (c)–(f) indicates areas where the difference is not statistically significant at the 90% level according to a Student's *t* test.

in interannual variability from CLM4.5 to VAR is due to the reduction of the number of soil layers when the model bedrock is shallow.

b. *Changes in the mean annual cycle*

Figure 5 explores the changes in mean annual cycle by looking at the mean annual range of the difference in the quantities surface runoff and baseflow between two runs [i.e., MAR(DEEP − CLM4.5), MAR(VAR − CLM4.5), or MAR(VAR − DEEP)]. Note that this MAR of the difference between two simulations is maximized when there is a magnitude change in or a temporal phase shift in the mean annual cycle. If neither of these occur, this statistic can be zero as indicated in the medians for 5 layers for surface runoff (Fig. 5a) and for 5, 6, and 14 layers for baseflow (Fig. 5b). The median for MAR(DEEP − CLM4.5) of surface runoff is approximately 0.07 mm day^{-1} where there are more than six soil layers in VAR. The median for MAR(VAR − CLM4.5) is similar to MAR(DEEP − CLM4.5) where the number of soil layers in VAR is greater than 10, while MAR(VAR − CLM4.5) is higher than that of MAR(DEEP − CLM4.5) where the number of soil layers is not changed or decreased in VAR (Fig. 5a). This suggests that the change in the mean annual cycle is due largely to the change in bottom boundary where the bedrock is deep (i.e., soil layers increased), whereas the reduced soil thickness in VAR adds to the annual cycle changes where the bedrock is shallow (i.e., soil layers $\leq$10). Similar to surface runoff, MAR(VAR − CLM4.5) and MAR(DEEP − CLM4.5) in baseflow are similar where the number of soil layers is greater than 10, but MAR(VAR − CLM4.5) $\gg$ MAR(DEEP − CLM4.5) for areas where the bedrock is shallow (Fig. 5b). The MAR(DEEP − VAR) for both surface runoff and baseflow is of a similar magnitude to MAR (VAR − CLM4.5) for shallow model bedrock but decreases to zero where DEEP and VAR are the same for 14 soil layers (Figs. 5a,b). This suggests that, where the model soil column is shallow, the differences between VAR and CLM4.5 is due to or added by the soil column being shallower than in CLM4.5, whereas most of the change between VAR and CLM4.5, where the bedrock is deep, is simply due to the change in bottom boundary condition imposed also in DEEP.

These changes to the mean annual cycle may be best illustrated at select locations (Table 1). First, we will consider five locations where the number of soil layers is less than 10 (i.e., shallow model bedrock). The annual cycle in latent heat (LH) flux (not shown) largely matches that of rainfall (Fig. S3 in the supplemental material) so that there can be no phase shift in LH flux in DEEP or VAR. This may not be the case if coupled to an atmospheric model because of potential feedbacks between LH flux and precipitation. Several studies (Anyah et al. 2008; Jiang et al. 2009; Leung et al. 2011) have shown changes to LH flux in response to changes in precipitation caused by the inclusion of groundwater models. At Karakoram and southeastern Africa, LH flux in DEEP is almost the same as in CLM4.5, whereas LH flux in VAR is as much as about 12 W m^{-2} lower than in DEEP and CLM4.5 (Figs. S4a,b in the supplemental material).

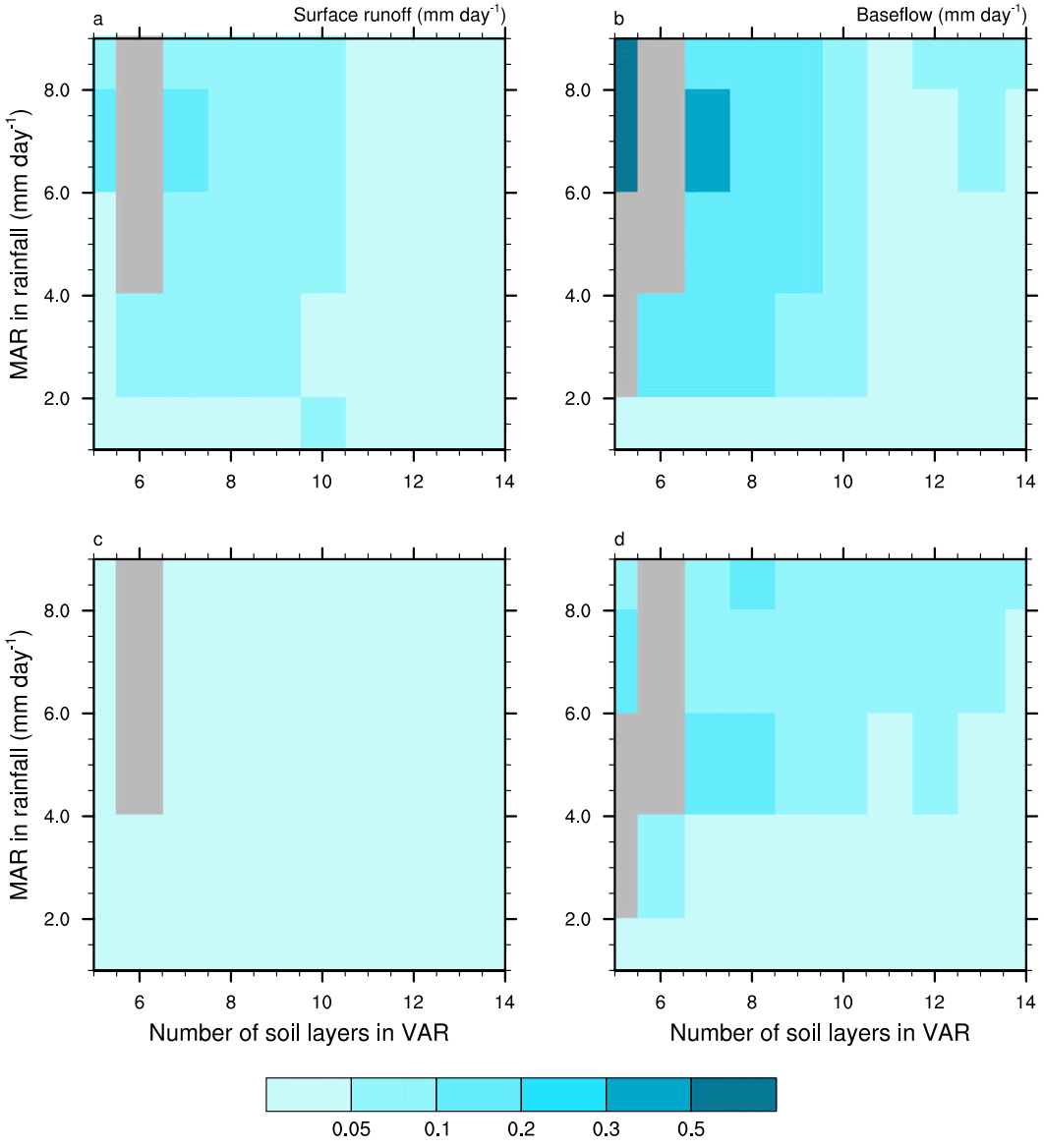

FIG. 4. The median root-mean-square difference (mm day^{-1}) (a),(b) between VAR and CLM4.5 and (c),(d) between DEEP and CLM4.5 in (left) surface runoff and (right) baseflow for every 2 mm day^{-1} bin of the mean annual range in rainfall and every number of soil layers to bedrock allowed in VAR. The gray areas denote bins with no data.

Temporal phase shifts are also not present in surface runoff at these five locations (Figs. 6a–c and Figs. S4e,f). DEEP tends to have a slightly smaller MAR at these locations with near-zero runoff at the southeastern Africa location. On the other hand, VAR generally has a higher maximum runoff at these locations (Figs. 6a–c) with the largest change in maximum runoff of approximately 0.37 mm day^{-1} occurring in southeastern Africa in February (Fig. S4b). In eastern Siberia, CLM4.5 and DEEP both produce peak runoff in late summer or early autumn with a secondary peak in the snowmelt season in May. DEEP decreases this secondary peak, but VAR increases it such that May is the month of maximum runoff in this run while maintaining similar runoff in late summer (Fig. 6b).

There are clear phase shifts in baseflow to earlier maximums in VAR at some locations (Figs. 6d–f). In the Yukon, DEEP reduces baseflow from CLM4.5, and VAR shifts it earlier (Fig. 6d). On the other hand, Southeast Asia baseflow is first increased by the bottom boundary condition change (i.e., DEEP) and then shifted earlier by variable soil thickness (i.e., VAR) (Fig. 6f).

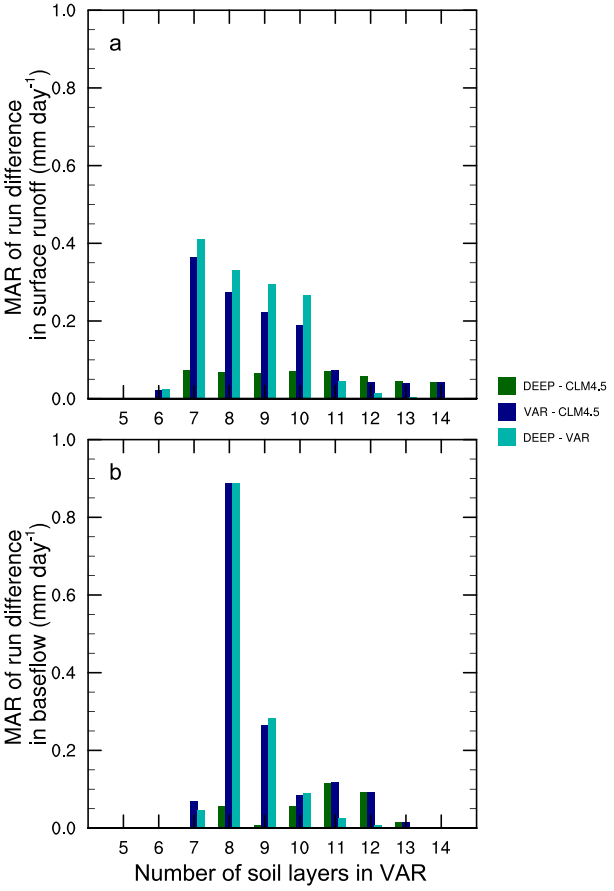

FIG. 5. The median MAR of the difference in (a) surface runoff and (b) baseflow between DEEP and CLM4.5 (i.e., DEEP − CLM4.5), between VAR and CLM4.5 (i.e., VAR − CLM4.5), and between DEEP and VAR (i.e., DEEP − VAR) for the number of soil layers used in VAR. A zero value of this statistic indicates that there is no change in the amplitude of or a temporal phase shift in the mean annual cycle.

TABLE 1. The sample locations referred to in Figs. 6, 7, and 8.

Location	Lat	Lon	No. of soil layers above bedrock in VAR
Karakoram	36.3°N	76.3°E	5
Yukon	62.5°N	129.5°W	7
Eastern Siberia	60.0°N	120.0°E	9
Southeastern Asia	20.0°N	102.0°E	8
Southeastern Africa	31.0°S	27.5°E	9
Chattanooga, Tennessee	35.0°N	85.3°W	10
Boulder, Colorado	40.0°N	105.3°W	13
Lower Mississippi River valley	35.0°N	93.0°W	14
Amazon	4.5°S	69.0°W	14
Tucson, Arizona	32.2°N	110.9°W	14

Infiltration (solid lines) and snowmelt (dashed lines) from the three runs are compared in the bottom row of Fig. 6 and Fig. S4. DEEP produces similar snowmelt and infiltration to CLM4.5 at all locations. On the other hand, the springtime peaks in surface runoff (Fig. 6a) and infiltration (Fig. 6g) are due to snowmelt in the Yukon. In the Yukon, snowmelt in VAR is reduced in April and enhanced in May, suggesting a delay in snowmelt with variable soil thickness. The increases in VAR surface runoff at all locations result in reduced infiltration, whereas DEEP infiltration is similar to CLM4.5's, especially in eastern Siberia and Southeast Asia. This suggests that the change in bottom boundary conditions has little effect on these quantities, but variable soil thickness does.

These changes to the water fluxes in the experimental simulations are clearly evidence or a result of soil moisture changes. The change in soil moisture θ in VAR relative to CLM4.5 for the latter four of the five shallow bedrock locations is shown in Figs. 7a–d, and the corresponding change in the saturation fraction θ/θ_{sat} (where θ_{sat} is soil porosity determined based on the soil texture, which is not uniform throughout the column) is presented in Figs. 7h–k. Soil moisture and saturation fraction are very much affected at these locations with shallow bedrock in VAR (Figs. 7a–d,h–k), but the annual cycle of soil moisture changes depends on location. In the Yukon (Figs. 7a,h), the soil column generally becomes wetter in the VAR simulation. On the other hand, in Siberia (Figs. 7b,i), the soil column generally becomes drier. Both locations have similar annual rainfall, but snowfall is less in Siberia than in the Yukon (Figs. S3b,c). The lower snowfall in Siberia results in lower infiltration during the snowmelt season, which is further reduced in VAR (Fig. 6h), drying out the soil column in that run. Snowfall is comparable in the Karakoram to that in the Yukon (Figs. S3a,b), but the snowmelt maximum is lower at Karakoram as a result of snowmelt occurring over an extended period (Fig. 6g and Fig. S4i). Thus, the moisture profile at Karakoram is also generally drier throughout the year except during the snowmelt maximum in March (not shown). For Southeast Asia (Fig. S3d), where there is a higher amplitude of the annual cycle of rainfall, the soil moisture amplitude is enhanced in VAR (Figs. 7c,j) with a drier springtime dry tongue and wetter wet tongues throughout the rest of the year. In South Africa, where there is less rainfall overall (Fig. S3e), the soil column gets drier in VAR (Figs. 7d,k) as a result of the decreased infiltration (Fig. S4j) resulting from the increased surface runoff (Fig. S4f). Many of these soil moisture changes at these shallow bedrock locations are statistically significant at the 90% level (Figs. 7a–d,h–k).

Interestingly, the moisture response in DEEP relative to CLM4.5 (Fig. S5 in the supplemental material) also

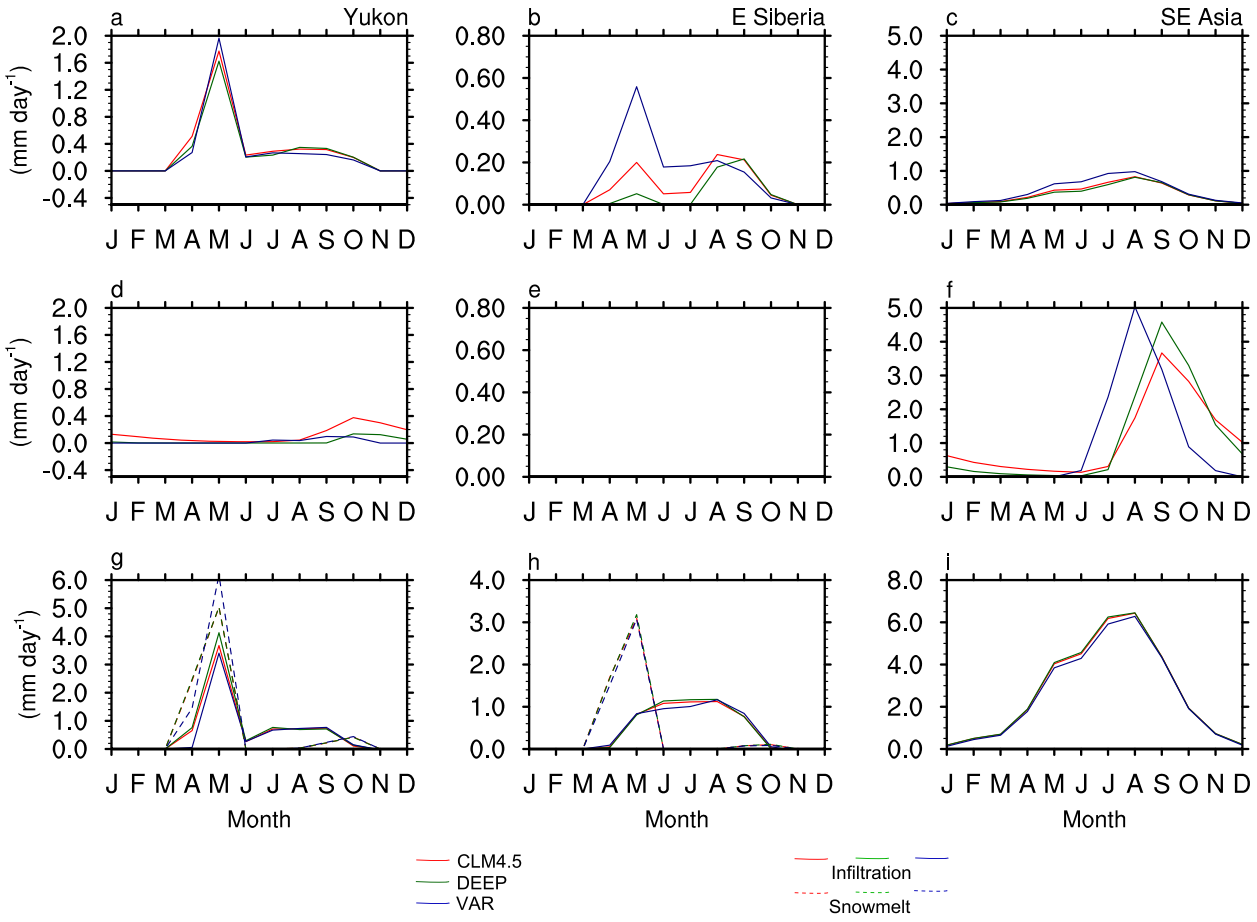

FIG. 6. The gridcell mean annual cycles in (a)–(c) surface runoff, (d)–(f) baseflow, and (g)–(i) infiltration and snowmelt simulated by CLM4.5, DEEP, and VAR for the first three locations in Table 1 where the number of soil layers is reduced from the CLM4.5 original 10 layers.

depends on location. The soil columns in the Yukon and eastern Siberia become slightly wetter throughout the year in all layers (Figs. S5a,b,f,g), whereas most of the soil column is changed very little throughout the year in Southeast Asia and southeastern Africa (Fig. S5c,d,i,j). Except at the eastern Siberian site, less of these moisture changes are statistically significant at the 90% level. Therefore, most of the soil moisture response seen in Figs. 7a–d,h–k is due to the change in soil thickness as seen in the change in soil moisture in VAR relative to DEEP (Fig. S6 in the supplemental material).

The horizontal lines in Figs. 7h–k represent the mean annual cycle in water table depth (WTD) in CLM4.5 (red), DEEP (green), and VAR (blue). VAR does not produce an aquifer at any of these locations as represented by the constant WTD at model bedrock depth, whereas CLM4.5 utilizing the unconfined aquifer model does have a WTD within model bedrock at these locations (Figs. 7h–k). DEEP with its 14 layers everywhere generates an aquifer in the Yukon and Southeast Asia as represented by WTDs generated above the bottom of the fourteenth layer (<~28 m) (Figs. 7h,j). On the other hand, it does not produce one in eastern Siberia and southeastern Africa since the DEEP WTDs at these two locations are at the bottom of the fourteenth layer (Figs. 7i,k).

At Chattanooga and in the lower Mississippi River valley and the Amazon, the mean annual cycles of LH flux and surface runoff from VAR and DEEP are both very similar to CLM4.5 and, thus, not shown. Baseflow, however, is more substantially affected in the sensitivity runs (Figs. 8a–c). In the 10 soil layers at Chattanooga, the spring maximum is slightly lower than CLM4.5 in DEEP but very similar to CLM4.5 throughout most of the rest of the year. On the other hand, VAR's springtime maximum is a little higher, while baseflow in VAR is much lower than CLM4.5 and DEEP throughout summer (Fig. 8a). These baseflows seem to follow the patterns in aquifer recharge as indicated by the dotted lines in Fig. 8d. In the lower Mississippi River valley and the Amazon, VAR and DEEP both produce similarly

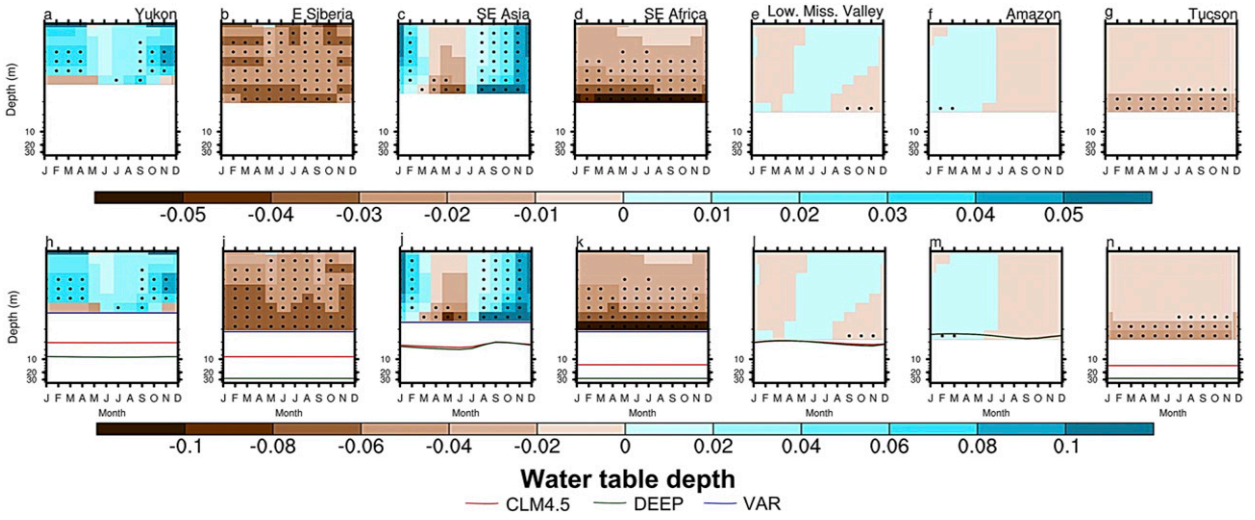

FIG. 7. The mean annual cycles of the change in (a)–(g) volumetric soil moisture content θ and (h)–(n) fraction of saturation θ/θ_{sat} in VAR from CLM4.5 for the grid cells containing 7 of the 10 locations in Table 1. Dots are given in each grid cell in which the difference is statistically significant at the 90% level according to a Student's t test. The horizontal lines in (h)–(n) represent the mean annual cycle in WTD in CLM4.5 (red), DEEP (green), and VAR (blue).

slightly higher maximum baseflow in boreal spring and lower minimum baseflow in boreal autumn at both locations (Figs. 8b,c). While maximum baseflow in the lower Mississippi River valley is slightly higher, it is preceded by larger winter baseflows as much as approximately 0.3 mm day^{-1}, and summer baseflows are lower by a similar amount (Fig. 8b). The higher boreal winter to spring baseflows are the result of more recharge to the aquifer, while the lower baseflows in summer and autumn are a result of less recharge to the

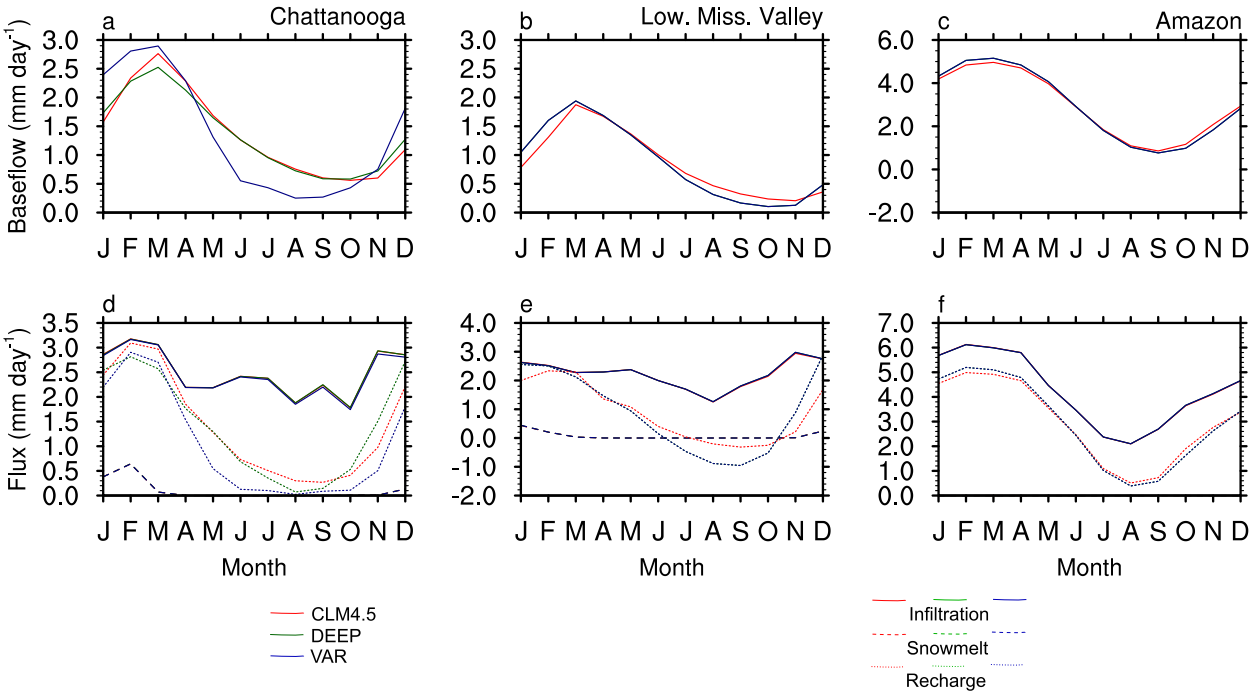

FIG. 8. The grid cell mean annual cycles in (a)–(c) baseflow and (d)–(f) infiltration, snowmelt, and recharge simulated by CLM4.5, DEEP, and VAR for three locations given in Table 1 where the number of soil layers is the same or increased from the CLM4.5 original 10 layers.

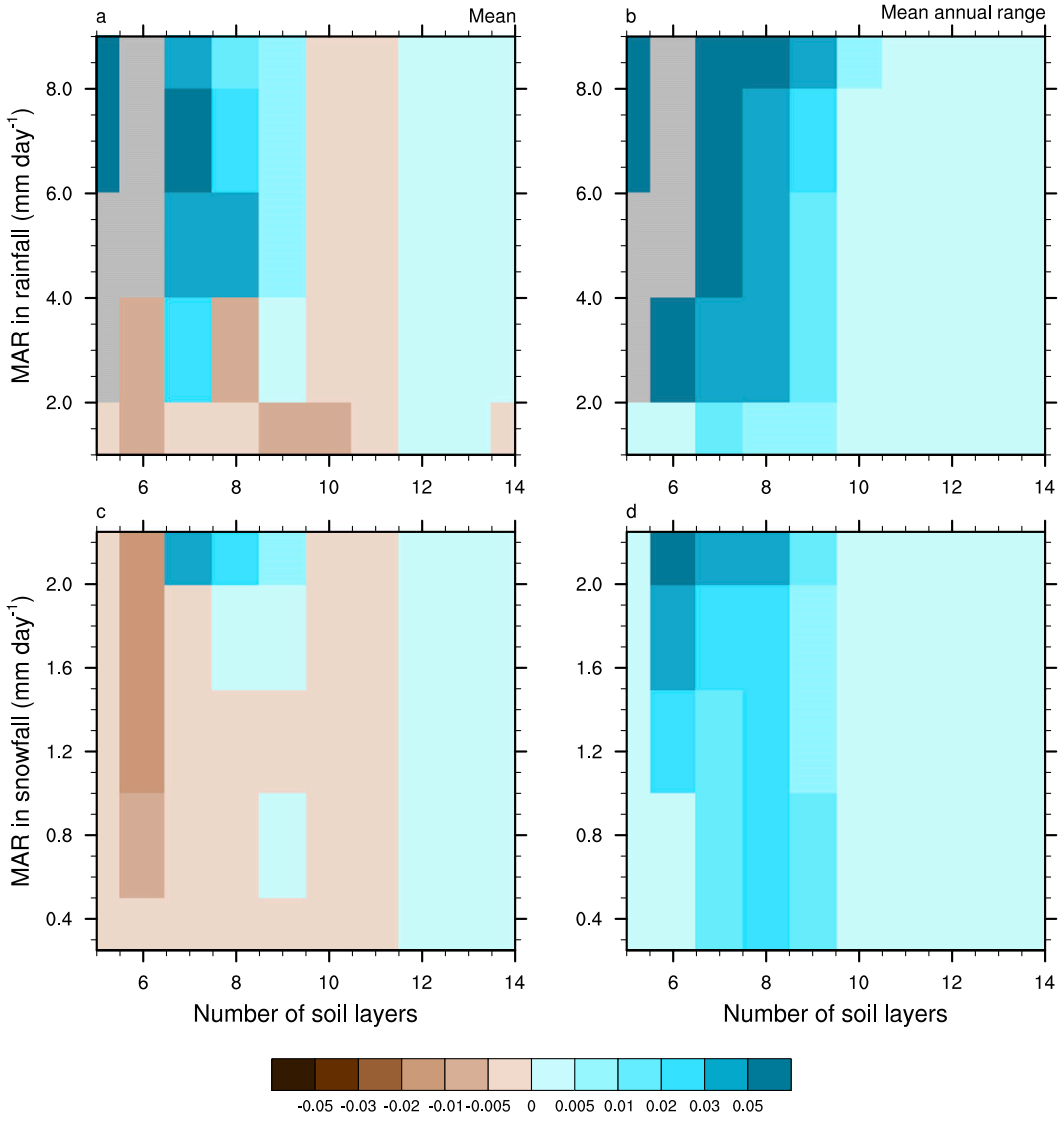

FIG. 9. The median change in the (a),(c) mean difference and the (b),(d) mean annual range in the difference in integrated top-five-layer (down to ~0.3 m) soil moisture between VAR and CLM4.5 for (top) 2 mm day^{-1} bins of the mean annual range in rainfall or (bottom) 0.5 mm day^{-1} bins of the mean annual range in snowfall and for every number of soil layers above bedrock allowed in VAR.

aquifer (Figs. 8e,f). These changes in DEEP and VAR relative to CLM4.5 in the lower Mississippi River valley and in the Amazon are a result of the change in the bottom boundary condition at these deep bedrock locations since these two simulations are exactly the same with the 14 soil layers at these two locations.

At the dry locations with deeper soil columns (Boulder and Tucson), LH flux (Figs. S4c,d) and baseflow (not shown) are not substantially changed as in the above three locations. Surface runoff is quite a bit lower in VAR and DEEP at these locations although not as much in VAR at Boulder (Figs. S4g,h).

Because of the above changes in recharge, WTD in the lower Mississippi River valley and the Amazon is slightly higher at the annual maximum and lower at the minimum. Otherwise, WTD is very similar in DEEP and VAR to that of CLM4.5 (Figs. 7l,m). Also, the simulated soil moisture in VAR is very similar to that of CLM4.5 (Figs. 7e,f,l,m), consistent with Gulden et al. (2007). Soil moisture changes in VAR are also similarly small in Chattanooga and Boulder (not shown). In the dry conditions of Tucson, the soil moisture profile in VAR is drier with slightly more drying in layers 9 and 10 (Figs. 7g,n). Since they both have 14 layers in the lower Mississippi

River valley, in the Amazon, and at Tucson, the soil moisture in DEEP and VAR is exactly the same, and the differences between the two are not shown.

To illustrate that variable soil thickness has more of an effect at locations with shallow bedrock than at those with deep bedrock applies globally, Fig. 9 shows the medians of the change in 1978–97 annual mean soil moisture content in the topmost five layers (down to ~0.3 m) in VAR from CLM4.5 and in the MAR of the difference between the two runs for various bins in the mean annual range in rainfall and snowfall as a function of the number of soil layers used in VAR. These topmost layers are of particular interest because they exist in every grid cell in VAR and interact most directly with the atmosphere. Figure 9 clearly shows that the soil moisture is most affected at locations where the number of soil layers is reduced. Since the change in these quantities in DEEP relative to CLM4.5 is small (not shown), most of this change is due to the reduction of soil layers used in VAR. Also, how much rain varies throughout the year has a greater impact on the mean annual cycle in soil moisture at shallow bedrock locations than does snowfall (Figs. 9a,c).

Figure 10a presents the median WTD difference between VAR and CLM4.5 when WTD is above model bedrock in VAR for various 2 mm day^{-1} wide bins of mean annual range of total precipitation. Where the number of soil layers has been increased beyond the 10 layers, WTD is less than 0.5 m different from CLM4.5. WTD can be within the soil column in VAR where the number of layers is 9 or 10 and can be >5 m lower (closer to the surface) than in CLM4.5 for nine soil layers. With a model bedrock depth of around 2.3 m, this means that CLM4.5 with the unconfined aquifer model places WTD below bedrock. No aquifer develops within the soil column in VAR for any fewer than nine soil layers, but one can see how much CLM4.5 WTDs are below model bedrock in the WTD difference between VAR and CLM4.5 for instances when there is no aquifer in VAR in Fig. 10b. CLM4.5 WTDs are below model bedrock in grid cells with 10 or fewer soil layers in VAR, being as high as 5 m or more below model bedrock where the soil column is shallow and the mean annual range of precipitation is small. For soil columns that have been extended in VAR, the WTD can actually be above the model bedrock in CLM4.5 when it does not actually develop in VAR as represented by the positive run differences here (Fig. 10b).

c. *Examples of regional changes*

To see how moisture changes on the regional scale, the monthly mean TWS anomalies from the model runs averaged over nine river basins across the globe are

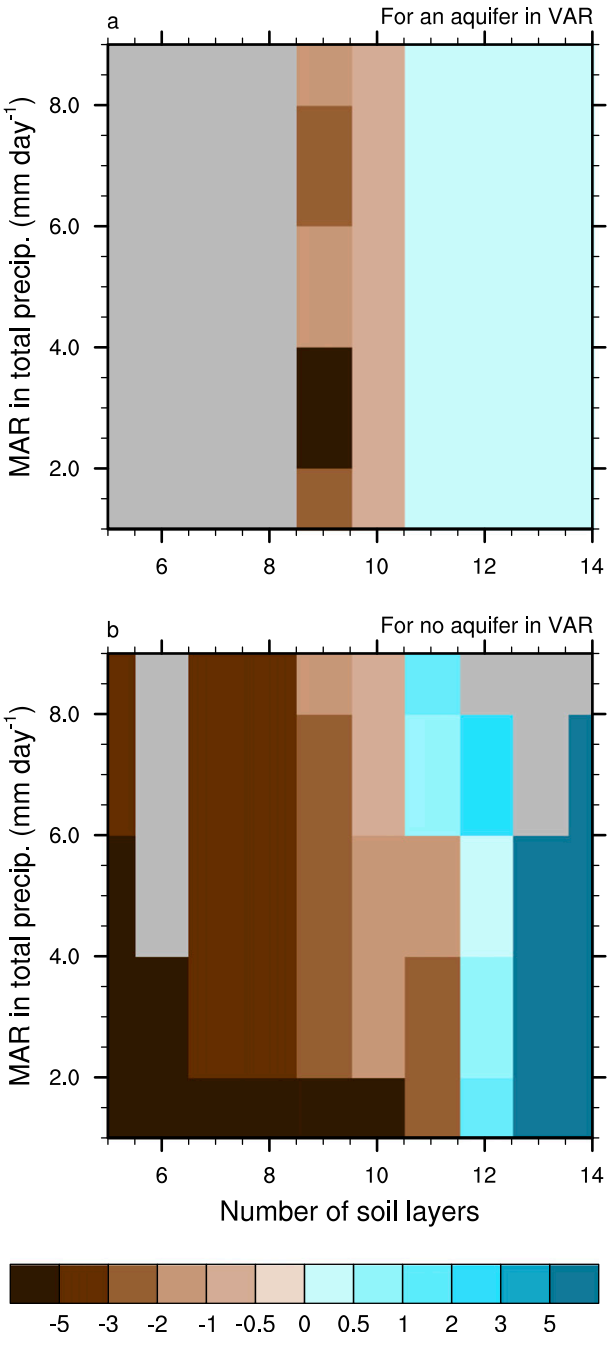

FIG. 10. The median difference in mean WTD between VAR and CLM4.5 for every 2 mm day^{-1} bin of the mean annual range in total precipitation and every number of soil layers to bedrock allowed in VAR for instances (a) when there is and (b) when there is not an aquifer in VAR. The negative values in (b) represent how much the WTD in CLM4.5 is theoretically below the model bedrock depth, while positive values indicate the existence of an aquifer in CLM4.5 when none exists in VAR.

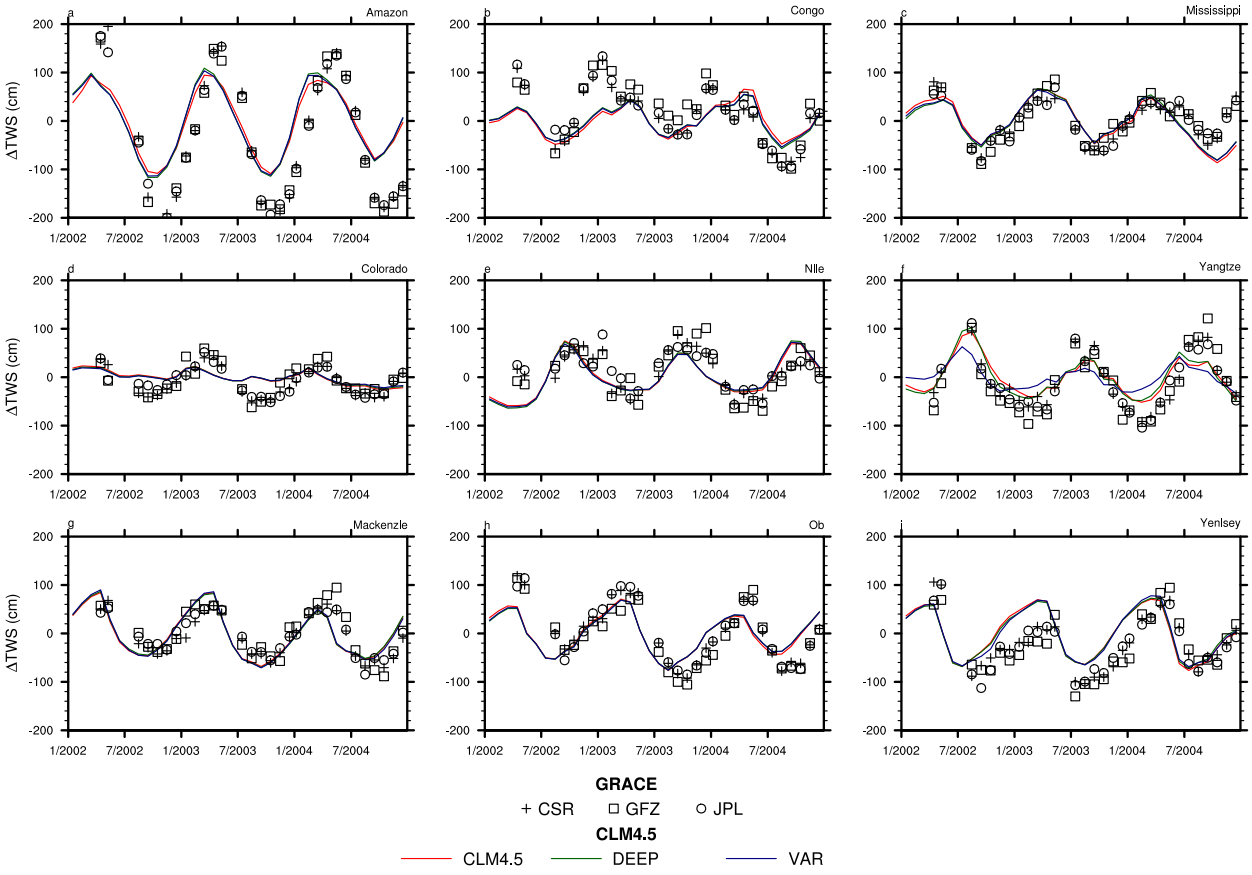

FIG. 11. The basin mean total water storage anomalies (ΔTWS) derived from GRACE measurements based upon the spherical harmonics from the Center for Space Research (CSR) at The University of Texas at Austin, GeoForschungsZentrum (GFZ) Potsdam, and the Jet Propulsion Laboratory (JPL) and as simulated by CLM4.5, DEEP, and VAR.

compared with those derived from GRACE measurements. Considering that a large fraction of these river basins are located mostly in lowlands with deep bedrock in the model, it is not surprising that the TWS anomalies are similar between DEEP and VAR for most river basins and that the difference in these from CLM4.5 is also small (Fig. 11). However, VAR TWS anomalies are dramatically different from CLM4.5's and DEEP's in the Yangtze River basin (Fig. 11f). Mountainous terrain with shallow model bedrock is included in a large portion of this basin. There are still problems with the model annual cycle of TWS such as the timing of peak storage or the lower annual range in TWS in the Colorado River basin (Fig. 11d) that the changes to the model implemented in VAR do not rectify.

Regional responses to rain events are also affected. Examples for rain events during June–August 1993 in the southwestern United States and northern Great Plains are given in section S2 of the supplemental material. The former region is more influenced by a decrease in soil column thickness since VAR's uppermost soil moisture is consistently lower than those from DEEP and CLM4.5. In the northern Great Plains, DEEP and VAR soil moisture are slightly higher than CLM4.5 on the day of rainfall, returning to CLM4.5 values within approximately 4 days (Fig. S8 in the supplemental material). VARCRU using the CRUNCEP forcing is also included in Fig. S8. The uppermost soil moisture in VARCRU is even lower than VAR's in the southwestern United States and lower than all the other runs in the northern Great Plains.

d. The effect on soil temperature

An additional effect of the inclusion of variable soil thickness in VAR is a change in the annual cycle of soil temperature globally. The mean annual range in soil temperature in CLM4.5 decreases with depth but still is as large as >4 K in some regions in the mid-to-high latitudes at the 12th node (Fig. 12a and Figs. S9a,b in the supplemental material). In much of the mid-to-high latitudes, the DEEP annual range in node 12 is reduced by as much as >2 K (Fig. 12b) in these same

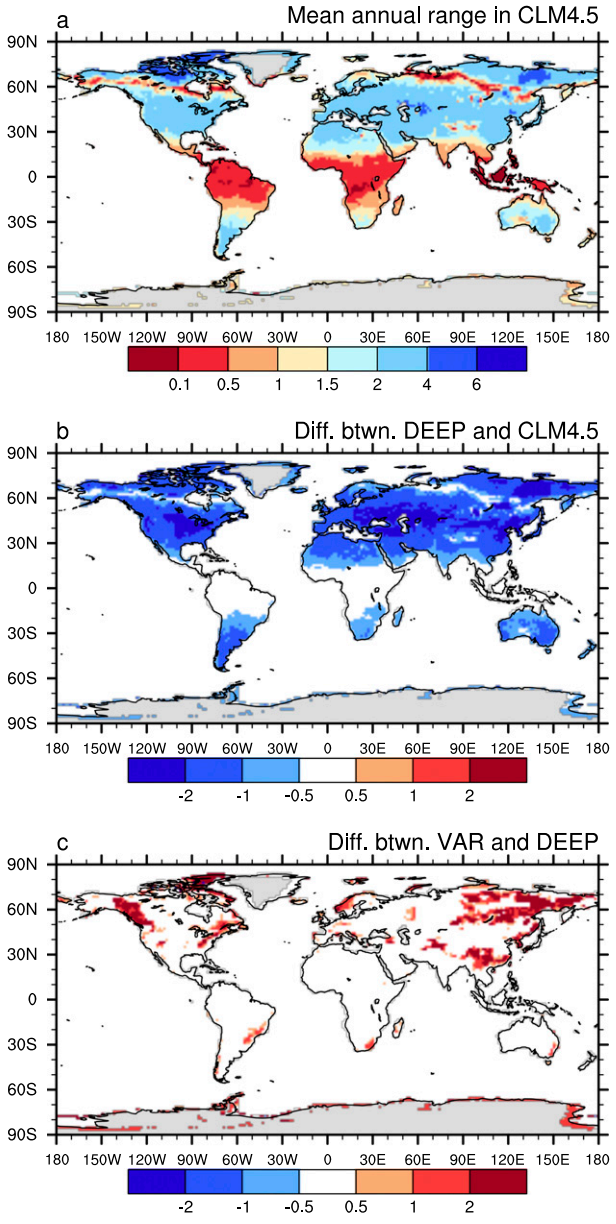

FIG. 12. (a) The mean annual range in soil temperature (K) in CLM4.5 and the difference in soil temperature mean annual range between (b) DEEP and CLM4.5 and (c) VAR and DEEP at node 12 (~7.9-m depth).

regions (Fig. 12a). This represents a substantial reduction in the annual cycle of temperature at this deep layer, which intuitively seems more realistic, as the annual cycle at such a depth is expected to be small.

The difference in mean annual range between VAR and DEEP, representing what is added by including variable soil thickness, is 0 everywhere the model bedrock is deep (Fig. 12c). Therefore, VAR retains the reduction in deep soil temperature annual range in these regions. However, the annual range in the whole column is increased in locations where the bedrock is shallower than the original 10 soil layers of CLM4.5 (Fig. 12c and Figs. S9e,f).

In those grid cells with deep bedrock necessitating adding soil layers to the original 10, the reduction of deep soil temperature annual range is caused by a reduction in heat capacity from that of granite/sandstone ($2.0 \times 10^6\,\mathrm{J\,m^{-3}\,K}$; Shabbir et al. 2000) to that of soil, which varies based on organic matter content and soil texture (Lawrence and Slater 2008). Thermal conductivity is also lowered from that of saturated granitic rock ($3.0\,\mathrm{W\,m^{-1}\,K^{-1}}$; Clauser and Huenges 1995) to that of soil (Farouki 1981). Of course, the opposite occurs in grid cells with shallow bedrock where the number of soil layers is reduced. Thus, the soil temperature annual cycle is increased throughout the column in places with shallow model bedrock and reduced substantially in deep soil throughout much of the mid-to-high latitudes where the model bedrock is deep (Figs. 12b,c and Fig. S9). Further changes in the soil temperature profile occur when adding water to the extra layers where the soil column is deepened. Changes also occur when removing water from soil layers where the soil column is made shallower.

This is further substantiated by comparing the single-point sensitivity simulations VARCV and VARTK with VAR in Fig. 13. The changes to VARCV of just the specific heat is minimal throughout the soil column and not statistically significant (Figs. 13c,d). When the thermal conductivity is also changed in VARTK, statistically significant changes are only made deeper, especially at the deeper soil site in the lower Mississippi River valley (Figs. 13e,f). The largest changes are made in VAR (Figs. 13g,h). At the shallower soil site in the Yukon (Fig. 13g), the soil temperature annual cycle is enhanced because the cold and warm tongues are stronger. The deep soil temperature is reduced at the deeper soil site in the lower Mississippi River valley (Fig. 13h) where the cold and warm tongues in the deeper layers are made slightly warmer and cooler. These changes in the deep layers are statistically significant. The soil water in VAR substantially enhances the changes made by just the specific heat in VARCV, whereas the thermal conductivity works in opposition to specific heat and the soil water, so the soil temperature profile changes in VAR would be even higher if it were not for thermal conductivity.

5. Discussion and conclusions

Variable soil thickness based upon a 30-arc-s dataset of the thickness of relatively porous, unconsolidated sediments over bedrock (Pelletier et al. 2016) has been

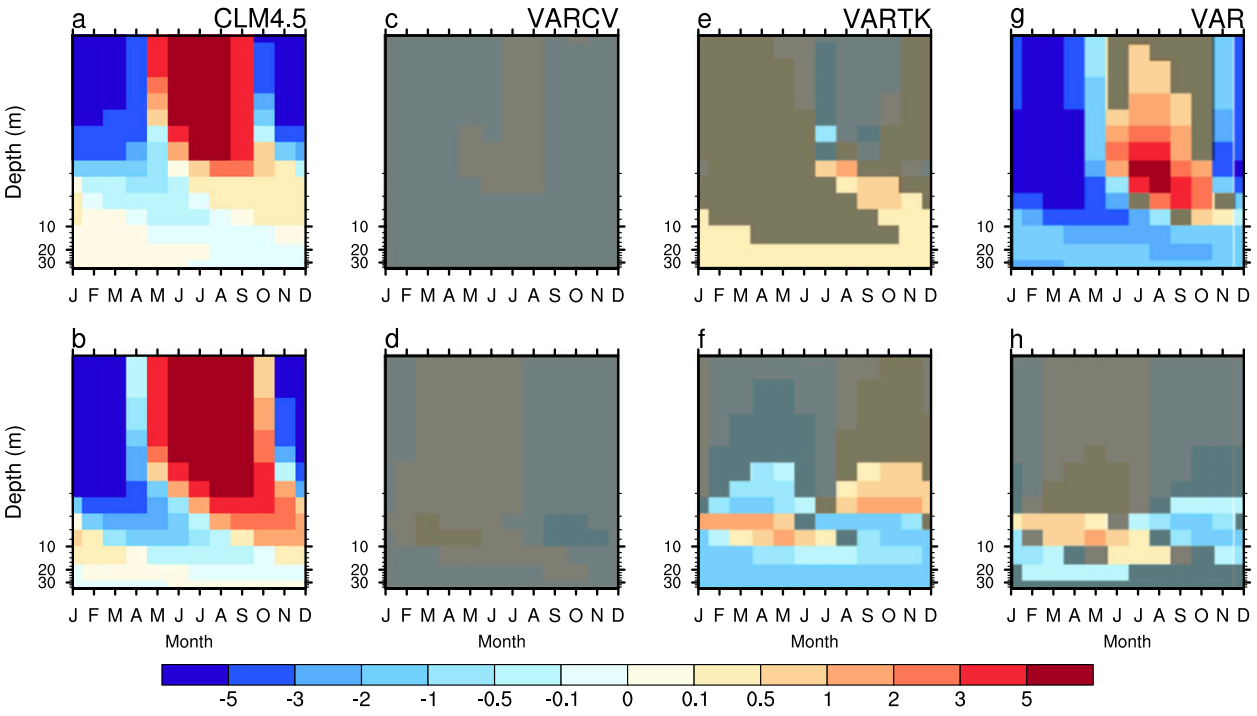

FIG. 13. (a),(b) The mean anomaly in soil temperature from the annual mean in CLM4.5 and the mean difference in soil temperature between (c),(d) VARCV, (e),(f) VARTK, and (g),(h) VAR from CLM4.5 in the grid cells containing the locations in Table 1 given for (top) the Yukon and (bottom) the lower Mississippi River valley. The contours for the anomalies in (a),(b) and the differences in (c)–(h) are the same. The overshading in (c)–(h) indicates areas where the difference is not statistically significant at the 90% level according to a Student's *t* test.

tested in version 4.5 of the Community Land Model (CLM4.5). Including variable soil thickness affects the model the most in locations with shallow bedrock (i.e., where the number of soil layers is reduced). The largest impact is to the mean annual range of the difference in quantities like surface runoff and baseflow in the simulation with variable soil depth (VAR) and the original version with a constant 10 layers atop an unconfined aquifer (CLM4.5) and in the root-mean-square difference between the two simulations representing the interannual variability. Baseflow is also affected in some grid cells where the number of soil layers actually increases, whereas surface quantities like latent heat flux and surface runoff are only substantially changed where the model bedrock is shallow.

The mean annual range of the simulation differences represents changes in the amplitude of the annual cycle as well as phase shifts in the annual cycle. There are no phase shifts in latent heat flux and surface runoff, so changes in these quantities are only limited to amplitude changes. However, there can be a change in the time of maximum baseflow in mountainous areas with shallow bedrock.

VAR is compared to a sensitivity run (DEEP) with the same framework as VAR but with a constant 14 layers everywhere in order to help reveal that some of the changes in VAR are due to the change of the bottom boundary conditions implicit with the removal of the aquifer model. The removal of the unconfined aquifer and the change in bottom boundary condition to zero flux does impact the model simulation even in regions with greater soil thickness), though these changes are much more dramatic in locations where the number of soil layers is decreased because of the presence of shallow soil thickness.

These changes to the water fluxes at and below the surface can be explained by the column soil moisture changes. When the model bedrock is deep (allowing for additional soil layers), the soil moisture does not change much throughout the column in VAR and DEEP. Thus, it similarly simulates the water table depth at many of these deep bedrock locations, and latent heat flux and surface runoff in particular remain largely unchanged in most of the grid cells where this occurs. This is consistent with Gulden et al. (2007), who found that total column water storage was similarly simulated with the unconfined aquifer model and a 30-layer soil column in Illinois. Therefore, the unconfined aquifer model is not necessary in CLM4.5 to produce a realistic aquifer for

regions with deep bedrock as long as the model soil column is realistically thick since the Richards equation was adapted for use in both unsaturated and saturated conditions (Zeng and Decker 2009).

On the other hand, the unconfined aquifer model simulates a water table depth in CLM4.5 that is below the model bedrock in VAR throughout the year in locations where the number of soil layers is reduced to below nine, whereas VAR produces no aquifer at these locations. It is at these locations that soil moisture throughout the soil column is most affected, explaining the enhanced sensitivity of surface runoff and baseflow. The effect on soil moisture and surface runoff varies in these shallow bedrock grid cells depending on annual rainfall and snowfall. The soil column can actually become drier throughout most of the year if snowfall or rainfall is low. If the annual cycle of rainfall is large, the annual cycle of soil moisture is enhanced in VAR with wetter wet tongues and drier dry tongues.

The above changes in soil moisture help to explain why the mean total water storage (TWS) anomalies for 2002–04 over several river basins globally do not generally change much from CLM4.5 to either DEEP or VAR, because river basins contain a large number of grid cells with deep bedrock in VAR. VAR is quite different than DEEP and CLM4.5 in the Yangtze River basin, which does include more mountainous terrain with shallow bedrock, suggesting that variable soil thickness would have more of an effect on basins largely within such terrain.

An added benefit of implementing variable soil depth is a change in the soil temperature annual cycle. For those grid cells with deep bedrock, which necessitates adding soil layers to the original 10 layers, the heat capacity of the layer is reduced from that of granite/sandstone (Shabbir et al. 2000) to that of soil, which varies based on organic matter content and soil texture (Lawrence and Slater 2008), and thermal conductivity is similarly reduced from that of granitic rock (Clauser and Huenges 1995) to that of soil (Farouki 1981). Of course, the opposite occurs in grid cells with shallow bedrock where the number of soil layers is reduced. Thus, the soil temperature annual cycle is increased throughout the column in places with shallow model bedrock and reduced substantially in deep soil throughout much of the mid-to-high latitudes where the model bedrock is deep. Specific heat has a minimal effect on the soil temperature profiles at two locations, one where the number of soil layers should be reduced (Yukon) and another where the number of soil layers should be increased (lower Mississippi River valley), as seen in a sensitivity run with just a change to the specific heat (VARCV). There is more of an effect with the addition of thermal conductivity in VARTK at the two locations, but the largest impact is made with the changes to the soil moisture profiles in VAR.

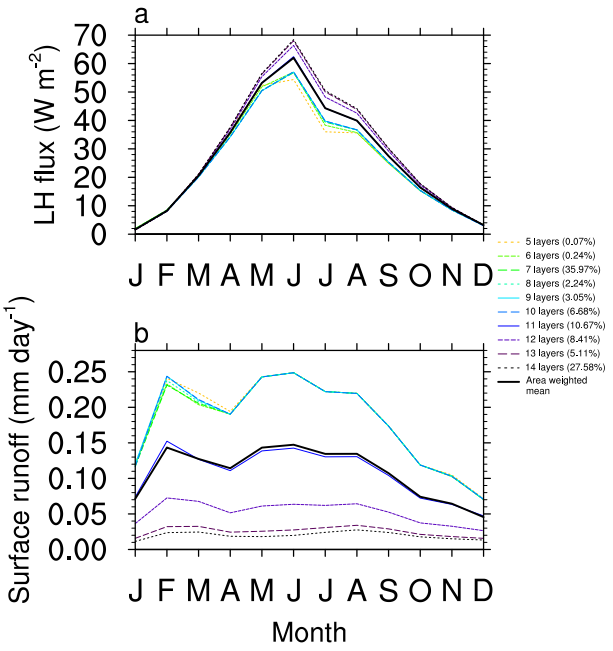

FIG. 14. The variation in (a) LH flux and (b) surface runoff from single-column simulations at 40.05°N, 105°W for all of the number of soil layers possible from the 30-arc-s data within the 0.9° lat × 1.25° lon grid cell (colored lines) and the area-weighted mean of these different simulations (dark black line). The soil depths for each of these number of layers can be found in Table S1.

It is important to note some caveats here. The model bedrock depth in VAR has been determined from the dataset soil thicknesses averaged to 0.9° latitude × 1.25° longitude used here, so unless much of a model grid box contains mountainous terrain, the shallow soil thicknesses found in that terrain will be averaged out with the deeper soil thickness of the valley bottoms. This could have important implications in basins where the hydrologic response is dominated by processes such as snowmelt in the headwaters. Perhaps this might be reduced when going to finer horizontal resolution in the land model or by including multiple columns within a grid cell each with its own soil thickness similar to what is already done for multiple vegetation covers in the model. Then, the gridcell mean quantities would be derived from the area-weighted means of the column values. A sample of what this might look like is given in Fig. 14 for the single grid cell at 40.05°N, 105°W containing Boulder, Colorado. The number of soil layers derived from the 30-arc-s soil thicknesses range across all allowed in VAR (5–14 layers; see Table S1 for the depths of these). There is a large spread in latent heat

fluxes simulated for the single column from spring into autumn with the largest spread of about 12 W m^{-2} occurring in June (colored lines in Fig. 14a). The spread in surface runoff between the various layer numbers occurs throughout the year (Fig. 14b). The area-weighted mean of these is given as the thick black line in Fig. 14; this is similar to the results for 11 layers. The number of layers as derived from the grid cell mean DTB is 11, whereas that derived from the median DTB is 9. The former produces LH fluxes and surface runoff closest to the area-weighted mean. The best way to characterize this subgrid variability in soil thickness will be the focus of future research. One possible way to do this would be to discriminate specifically between vertical and lateral processes. The former would be solved at the grid scale, while the latter would be performed at a much higher resolution. Recently, Hazenberg et al. (2015) have shown that such a hybrid three-dimensional approach performs well at the hillslope scale, and this method is currently being extended to account for lateral flow within hillslopes, riparian zones, and valley bottoms.

The interaction between the atmosphere and land is also ignored here by running CLM4.5 offline with the Qian et al. (2006) forcing. Recent research has shown that a model atmosphere would respond to groundwater dynamics (Anyah et al. 2008; Jiang et al. 2009; Leung et al. 2011). Using a different forcing, CRUNCEP in VARCRU, also has an effect on the variable soil thickness simulation as seen by the drier uppermost soil moisture in the southwestern United States and the northern Great Plains in Fig. S8. Even so, the changes to basin TWSs is minimal in VARCRU (not shown). There are very large changes in VARCRU surface runoff and baseflow from that of VAR in the same regions where VAR seemed to have the most effect on these quantities (Fig. S11 in the supplemental material). In some regions, the changes in VARCRU counteract those made by VAR from CLM4.5. Still, most of these largest differences from VAR are statistically significant at the 90% level.

Furthermore, the effects of deep roots are ignored by limiting the roots to the 10th layer in VAR. However, deep roots have been observed down to around 18 m in the Amazon (Nepstad et al. 1994), and deep roots may be particularly important in arid and semiarid regions (Canadell et al. 1996). To test how important this is, we perform an additional sensitivity test that is the same as VAR except that root fractions are allowed in all layers. The latent heat fluxes from this sensitivity run are within ± 1 W m^{-2} of VAR's everywhere, the difference of which is not statistically significant at the 90% level anywhere (Fig. S10 in the supplemental material). The effects of deep roots may be minimized here because of the formulation of root fraction used in CLM4.5. Root fraction exponentially decays with depth, so root fractions are very small at depth. This may need to be adjusted for the deeper soil columns allowed with variable soil thickness. Another possibility is that the deep roots serve to move water up during dry periods and down during wet periods via hydraulic redistribution. Lee et al. (2005) showed that the inclusion of this process improved the simulation of climate over the Amazon in CLM coupled to the Community Atmosphere Model. However, Romero-Saltos et al. (2005) observed that water moved upward during dry periods in the Amazon through the soil rather than through the roots. The impacts of land–atmosphere feedbacks and deep root distributions should be explored further using variable soil depth in LSMs.

Still, the model is made more realistic with the inclusion of variable soil thickness on the coarse gridcell scale used here because soil thickness is known to vary between uplands and lowlands. The use of unconfined aquifer models in which groundwater is partially separate from the soil column was necessitated by the implementation of constant soil thicknesses in CLM because of the previous lack of sufficient information to establish a reasonable estimate of soil thickness. Because of the use of Zeng and Decker's (2009) revised Richards equation in CLM, VAR has similar water table depths to those in CLM4.5 in areas where the bedrock is deep. However, in some cases, the CLM4.5 aquifer model generates water table depths below bedrock in locations with shallow soil thicknesses, whereas no aquifer is able to exist in VAR. Therefore, this implementation of variable soil thickness represents a step forward in LSM development that might have more of an impact at higher resolution or when the subgrid variability in soil thickness can be represented.

Acknowledgments. This work was supported by DOE (DE-SC0006773), NASA (NNX13AK82A), and NSF (AGS-0944101). L. R. Leung was supported by the DOE Office of Science Biological and Environmental Research Earth System Modeling program. Pacific Northwest National Laboratory is operated for DOE by Battelle Memorial Institute under contract DE-AC05-76RL01830. We thank the Jet Propulsion Laboratory for providing the GRACE data, which were processed by Sean Swenson under support from the NASA MEaSUREs Program. High-performance computing support was provided by NCAR's Computational and Information Systems Laboratory, sponsored by the National Science Foundation, through computing time on Yellowstone (http://n2t.net/ark:/85065/d7wd3xhc) and on The University of Arizona Research Computing

High Performance Computing and High Throughput Computing system.

REFERENCES

Anyah, R. O., C. P. Weaver, G. Miguez-Macho, Y. Fan, and A. Robock, 2008: Incorporating water table dynamics in climate modeling: 3. Simulated groundwater influence on coupled land-atmosphere variability. *J. Geophys. Res.*, **113**, D07103, doi:10.1029/2007JD009087.

Canadell, J., R. B. Jackson, J. R. Ehleringer, H. A. Mooney, O. E. Sala, and E.-D. Schulze, 1996: Maximum rooting depth of vegetation types at the global scale. *Oecologia*, **108**, 583–595, doi:10.1007/BF00329030.

Chen, J. L., M. Rodell, C. R. Wilson, and J. S. Famiglietti, 2005: Low degree spherical harmonic influences on Gravity Recovery and Climate Experiment (GRACE) water storage estimates. *Geophys. Res. Lett.*, **32**, L14405, doi:10.1029/2005GL022964.

Chen, X., and Q. Hu, 2004: Groundwater influences on soil moisture and surface evaporation. *J. Hydrol.*, **297**, 285–300, doi:10.1016/j.jhydrol.2004.04.019.

Clauser, C., and E. Huenges, 1995: Thermal conductivity of rocks and minerals. *Rock Physics and Phase Relations: A Handbook of Physical Constants*, T. J. Ahrens, Ed., Amer. Geophys. Union, 105–126.

Decker, M., and X. Zeng, 2009: Impact of modified Richards equation on global soil moisture simulation in the Community Land Model (CLM3.5). *J. Adv. Model. Earth Syst.*, **1**, 5, doi:10.3894/JAMES.2009.1.5.

Dietrich, W. E., R. Reiss, M.-L. Hsu, and D. R. Montgomery, 1995: A process-based model for colluvial soil depth and shallow landsliding using digital elevation data. *Hydrol. Processes*, **9**, 383–400, doi:10.1002/hyp.3360090311.

Eltahir, E. A. B., and P. J.-F. Yeh, 1999: On the assymetric response of aquifer water level to floods and droughts in Illinois. *Water Resour. Res.*, **35**, 1199–1217, doi:10.1029/1998WR900071.

Fan, Y., H. Li, and G. Miguez-Macho, 2013: Global patterns of groundwater table depth. *Science*, **339**, 940–943, doi:10.1126/science.1229881.

Farouki, O. T., 1981: The thermal properties of soils in cold regions. *Cold Reg. Sci. Technol.*, **5**, 67–75, doi:10.1016/0165-232X(81)90041-0.

Gochis, D. J., E. R. Vivoni, and C. J. Watts, 2010: The impact of soil depth on land surface energy and water fluxes in the North American monsoon region. *J. Arid Environ.*, **74**, 564–571, doi:10.1016/j.jaridenv.2009.11.002.

Gulden, L. E., E. Rosero, Z.-L. Yang, M. Rodell, C. S. Jackson, G.-Y. Niu, P. J.-F. Yeh, and J. Famiglietti, 2007: Improving land-surface model hydrology: Is an explicit aquifer model better than a deeper soil profile? *Geophys. Res. Lett.*, **34**, L09402, doi:10.1029/2007GL029804.

Gutowski, W. J., C. J. Vörösmarty, M. Person, Z. Ötles, B. Fekete, and J. York, 2002: A coupled land-atmosphere simulation program (CLASP): Calibration and validation. *J. Geophys. Res.*, **107**, 4283, doi:10.1029/2001JD000392.

Hazenberg, P., Y. Fang, P. Broxton, D. Gochis, G.-Y. Niu, J. D. Pelletier, P. A. Troch, and X. Zeng, 2015: A hybrid-3D hillslope hydrological model for use in Earth system models. *Water Resour. Res.*, **51**, 8218–8239, doi:10.1002/2014WR016842.

Jiang, X., G.-Y. Niu, and Z.-L. Yang, 2009: Impacts of vegetation and groundwater dynamics on warm season precipitation over the central United States. *J. Geophys. Res.*, **114**, D06109, doi:10.1029/2008JD010756.

Koirala, S., P. J.-F. Yeh, Y. Hirabayashi, S. Kanae, and T. Oki, 2014: Global-scale land surface hydrologic modeling with the representation of water table dynamics. *J. Geophys. Res. Atmos.*, **119**, 75–89, doi:10.1002/2013JD020398.

Landerer, F. W., and S. C. Swenson, 2012: Accuracy of scaled GRACE terrestrial water storage estimates. *Water Resour. Res.*, **48**, W04531, doi:10.1029/2011WR011453.

Lawrence, D. M., and A. G. Slater, 2008: Incorporating organic soil into a global climate model. *Climate Dyn.*, **30**, 145–160, doi:10.1007/s00382-007-0278-1.

Lee, J.-E., R. S. Oliveira, T. E. Dawson, and I. Fung, 2005: Root functioning modifies seasonal climate. *Proc. Natl. Acad. Sci. USA*, **102**, 17 576–17 581, doi:10.1073/pnas.0508785102.

Leung, L. R., M. Huang, Y. Qian, and X. Liang, 2011: Climate–soil–vegetation control on groundwater table dynamics and its feedbacks in a climate model. *Climate Dyn.*, **36**, 57–81, doi:10.1007/s00382-010-0746-x.

Liang, X., Z. Xie, and M. Huang, 2003: A new parameterization for surface and groundwater interactions and its impact on water budgets with the Variable Infiltration Capacity (VIC) land surface model. *J. Geophys. Res.*, **108**, 8613, doi:10.1029/2002JD003090.

Miguez-Macho, G., and Y. Fan, 2012: The role of groundwater in the Amazon water cycle: 1. Influence on seasonal streamflow, flooding and wetlands. *J. Geophys. Res.*, **117**, D15113, doi:10.1029/2012JD017539.

——, ——, C. P. Weaver, R. Walko, and A. Robock, 2007: Incorporating water table dynamics in climate modeling: 1. Water table observations and equilibrium water table simulations. *J. Geophys. Res.*, **112**, D13108, doi:10.1029/2006JD008112.

Miller, D. A., and R. A. White, 1998: A conterminous United States multilayer soil characteristics dataset for regional climate and hydrology modeling. *Earth Interact.*, **2**, 1–26, doi:10.1175/1087-3562(1998)002<0001:ACUSMS>2.3.CO;2.

Nepstad, D. C., and Coauthors, 1994: The role of deep roots in the hydrological and carbon cycles of Amazonian forests and pastures. *Nature*, **372**, 666–669, doi:10.1038/372666a0.

Niu, G.-Y., Z.-L. Yang, R. E. Dickinson, and L. E. Gulden, 2005: A simple TOPMODEL-based runoff parameterization (SIMTOP) for use in global climate models. *J. Geophys. Res.*, **110**, D21106, doi:10.1029/2005JD006111.

——, ——, ——, ——, and H. Su, 2007: Development of a simple groundwater model for use in climate models and evaluation with Gravity Recovery and Climate Experiment data. *J. Geophys. Res.*, **112**, D07103, doi:10.1029/2006JD007522.

Oleson, K. W., and Coauthors, 2013: Technical description of version 4.5 of the Community Land Model (CLM). NCAR Tech. Note NCAR/TN-503+STR, 420 pp. [Available online at http://www.cesm.ucar.edu/models/cesm1.2/clm/CLM45_Tech_Note.pdf.]

Orellana, F., P. Verma, S. P. Loheide II, and E. Daly, 2012: Monitoring and modeling water-vegetation interactions in groundwater-dependent ecosystems. *Rev. Geophys.*, **50**, RG2003, doi:10.1029/2011RG000383.

Pelletier, J. D., 2013: A robust, two-parameter method for the extraction of drainage networks from high-resolution digital elevation models (DEMs): Evaluation using synthetic and real-world DEMs. *Water Resour. Res.*, **49**, 75–89, doi:10.1029/2012WR012452.

——, and C. Rasmussen, 2009: Geomorphically based predictive mapping of soil thickness in upland watersheds. *Water Resour. Res.*, **45**, W09417, doi:10.1029/2008WR007319.

——, and Coauthors, 2016: A gridded global data set of soil, immobile regolith, and sedimentary deposit thicknesses for regional and global land surface modeling. *J. Adv. Model. Earth Syst.*, doi:10.1002/2015MS000526, in press.

Qian, T., A. Dai, K. E. Trenberth, and K. W. Oleson, 2006: Simulation of global land surface conditions from 1948 to 2004. Part I: Forcing data and evaluations. *J. Hydrometeor.*, **7**, 953–975, doi:10.1175/JHM540.1.

Roering, J. J., 2008: How well can hillslope evolution models "explain" topography? Simulating soil transport and production with high-resolution topographic data. *Geol. Soc. Amer. Bull.*, **120**, 1248–1262, doi:10.1130/B26283.1.

Romero-Saltos, H., L. da Silveira Lobo Sternberg, M. Z. Moreira, and D. C. Nepstad, 2005: Rainfall exclusion in an eastern Amazonian forest alters soil water movement and depth of water uptake. *Amer. J. Bot.*, **92**, 443–455, doi:10.3732/ajb.92.3.443.

Rossatto, D. R., L. de Carvalho Ramos Silva, R. Villalobos-Vega, L. da Silveira Lobo Sternberg, and A. C. Franco, 2012: Depth of water uptake in woody plants relates to groundwater level and vegetation structure along a topographic gradient in a neotropical savanna. *Environ. Exp. Bot.*, **77**, 259–266, doi:10.1016/j.envexpbot.2011.11.025.

Shabbir, G., A. Maqsood, and C. A. Majid, 2000: Thermophysical properties of consolidated porous rocks. *J. Phys.*, **33D**, 658–661, doi:10.1088/0022-3727/33/6/311.

Swenson, S. C., 2012: GRACE monthly land water mass grids NETCDF RELEASE 5.0. version 5.0. PO.DAAC, data accessed 11 December 2014, doi:10.5067/TELND-NC005.

——, and J. Wahr, 2006: Post-processing removal of correlated errors in GRACE data. *Geophys. Res. Lett.*, **33**, L08402, doi:10.1029/2005GL025285.

Tesfa, T. K., D. G. Tarboton, D. G. Chandler, and J. P. McNamara, 2009: Modeling soil depth from topographic and land cover attributes. *Water Resour. Res.*, **45**, W10438, doi:10.1029/2008WR007474.

Woolhiser, D. A., R. W. Fedora, R. E. Smith, and S. A. Stohoff, 2006: Estimating infiltration in the Upper Split Wash Watershed, Yucca Mountain, Nevada. *J. Hydrol. Eng.*, **11**, 123–133, doi:10.1061/(ASCE)1084-0699(2006)11:2(123).

Yeh, P. J.-F., and E. A. B. Eltahir, 2005: Representation of water table dynamics in a land surface scheme. Part I: Model development. *J. Climate*, **18**, 1861–1880, doi:10.1175/JCLI3330.1.

——, M. Irizarry, and E. A. B. Eltahir, 1998: Hydroclimatology of Illinois: A comparison of monthly evaporation estimates based on atmospheric water balance and soil water balance. *J. Geophys. Res.*, **103**, 19 823–19 837, doi:10.1029/98JD01721.

York, J. P., M. Person, W. J. Gutowski, and T. C. Winter, 2002: Putting aquifers into atmospheric simulation models: An example from the Mill Creek Watershed, northeastern Kansas. *Adv. Water Resour.*, **25**, 221–238, doi:10.1016/S0309-1708(01)00021-5.

Zeng, X., 2001: Global vegetation root distribution for land modeling. *J. Hydrometeor.*, **2**, 525–530, doi:10.1175/1525-7541(2001)002<0525:GVRDFL>2.0.CO;2.

——, and M. Decker, 2009: Improving the numerical solution of soil moisture–based Richards equation for land models with a deep or a shallow water table. *J. Hydrometeor.*, **10**, 308–319, doi:10.1175/2008JHM1011.1.

——, Y.-J. Dai, R. E. Dickinson, and M. Shaikh, 1998: The role of root distribution for climate simulation over land. *Geophys. Res. Lett.*, **25**, 4533–4536, doi:10.1029/1998GL900216.